AD-A129 323 USE OF HOLOGRAPHIC LINEAR FRINGE LINEARIZATION INTERFEROMETRY (FLI) FOR D..(U) HONEYWELL ELECTRO-OPTICS DIV LEXINGTON MA G O REYNOLDS ET AL. 1/1

UNCLASSIFIED APR 83 8303-22 AFOSR-TR-83-0464 F/G 20/6 NL

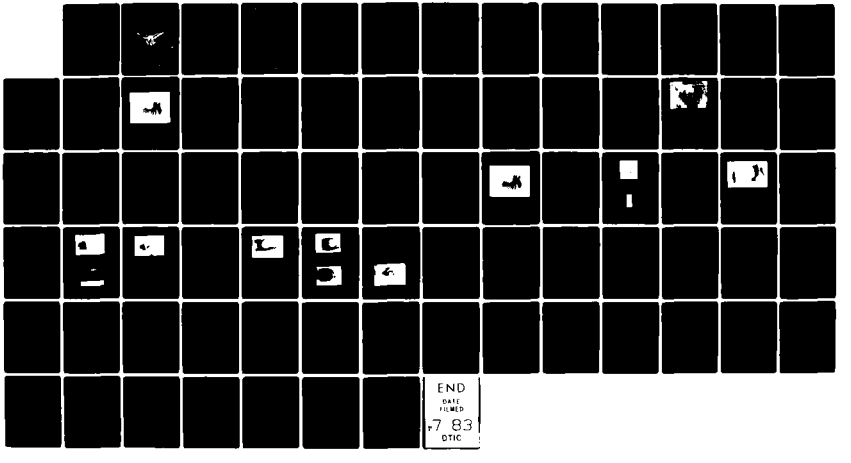

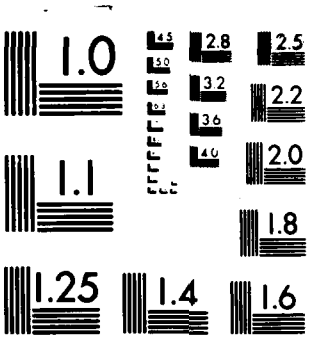

MICROCOPY RESOLUTION TEST CHART
NATIONAL BUREAU OF STANDARDS-1963-A

AFOSR-TR- 83-0464

8303-22

13

Use of Holographic Linear Fringe Linearization Interferometry (FLI) For Detection of Defects

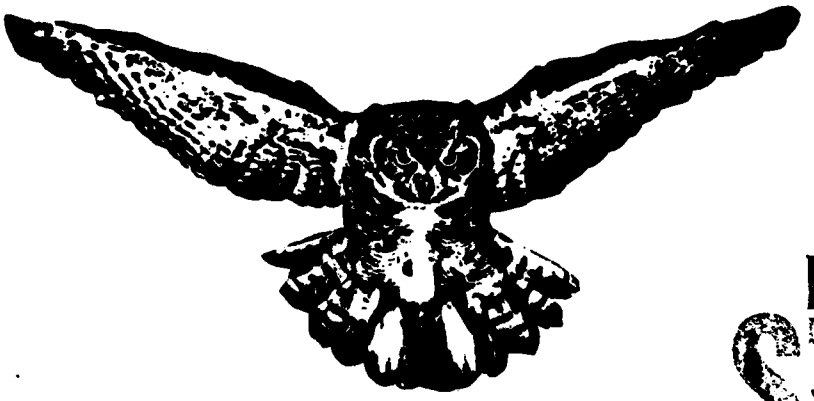

AD A129323

DTIC ELECTE JUN 1 0 1983 S D A

Approved for public release; distribution unlimited.

DTIC FILE COPY

Honeywell

83 06 10 001

8303-22

ANNUAL REPORT

on

Contract F49620-82-C-0001

USE OF HOLOGRAPHIC LINEAR FRINGE LINEARIZATION INTERFEROMETRY (FLI) FOR DETECTION OF DEFECTS

15 April 1983

Principal Investigator

GEORGE O. REYNOLDS

AIR FORCE OFFICE OF SCIENTIFIC RESEARCH (AFSC)
NOTICE OF TRANSMITTAL TO DTIC
This technical report has been reviewed and is
approved for public release IAW AFR 190-12.
Distribution is unlimited.
MATTHEW J. KERPER
Chief, Technical Information Division

Honeywell

ELECTRO-OPTICS DIVISION
2 Forbes Road
Lexington, MA 02173

UNCLASSIFIED

SECURITY CLASSIFICATION OF THIS PAGE (When Data Entered)

REPORT DOCUMENTATION PAGE	READ INSTRUCTIONS BEFORE COMPLETING FORM
1. REPORT NUMBER: AFOSR-TR- 83-0464 / 2. GOVT ACCESSION NO.: A129323	3. RECIPIENT'S CATALOG NUMBER
4. USE OF HOLOGRAPHIC LINEAR FRINGE LINEARIZATION INTERFEROMETRY (FLI) FOR DETECTION OF DEFECTS	5. TYPE OF REPORT & PERIOD COVERED: Annual Jan. 15, 1982 – Jan. 15, 1983
	6. PERFORMING ORG. REPORT NUMBER
7. George O. Reynolds, Principal Investigator, Donald A. Servaes, John B. DeVelis, Honeywell EOD & Ronald A. Mayville, Arthur D. Little, Inc.	8. CONTRACT OR GRANT NUMBER(s): F49620-82-C-0001
9. PERFORMING ORGANIZATION NAME AND ADDRESS: Honeywell Electro-Optics Division, 2 Forbes Road, Lexington, MA 02173	10. PROGRAM ELEMENT, PROJECT, TASK AREA & WORK UNIT NUMBERS: 61102F 2306/A2
11. CONTROLLING OFFICE NAME AND ADDRESS: USAF, AFSC, Air Force Office of Scientific Research, Bldg. 410, Bolling AFB, D.C. 20332	12. REPORT DATE: April 1983
	13. NUMBER OF PAGES: 72
14. MONITORING AGENCY NAME & ADDRESS(if different from Controlling Office)	15. SECURITY CLASS. (of this report): UNCLASSIFIED
	15a. DECLASSIFICATION/DOWNGRADING SCHEDULE: NA

16. DISTRIBUTION STATEMENT (of this Report)

Approved for public release; distribution unlimited.

17. DISTRIBUTION STATEMENT (of the abstract entered in Block 20, if different from Report)

18. SUPPLEMENTARY NOTES

19. KEY WORDS (Continue on reverse side if necessary and identify by block number)

Holographic Interferometry, Non-Destructive Evaluation, Lasers, Spatial Filtering, Fringe Localization

20. ABSTRACT (Continue on reverse side if necessary and identify by block number)

This report describes the progress during Phase I on the two step Holographic Fringe Linearization Interferometry (FLI) Study. The FLI process consists of deflecting the object beam between holographic exposures to create linear fringes and spatially filtering of the image reconstructed from the hologram to discriminate between subsurface defects and random fringe noise. The fringe localization procedures utilized to put the linear fringes on the surface of interest are

DD FORM 1 JAN 73 1473 EDITION OF 1 NOV 68 IS OBSOLETE

UNCLASSIFIED

SECURITY CLASSIFICATION OF THIS PAGE (When Data Entered)

UNCLASSIFIED

described. The design of the repeatable thermal deformation procedures used in the preliminary experiments are discussed. The design of both the holographic recording, reconstruction and spatial filtering systems are given. Preliminary experimental results show the separation of linear fringe information and random noise in the Fourier plane of the spatial filtering system. Various filter designs which enhance the images are also discussed. System feasibility is demonstrated for a triple exposure experiment in which controlled noise was added with a third exposure. Controlled loading experiments are shown to agree with the results predicted analytically with a simple bending finite element model. Plans for the work in Phase II are presented.

UNCLASSIFIED

TABLE OF CONTENTS

DTIC COPY INSPECTED 2

Accession For
NTIS
DTIC
Unannounced
Justification
By
Distribution
Availability Codes
Dist
A

APPENDICES

LIST OF ILLUSTRATIONS

LIST OF ILLUSTRATIONS (Contined)

LIST OF TABLES

SECTION 1
INTRODUCTION

This report describes the progress during Phase I on Contract F49620-82-C-0001 entitled "Use of Holographic Fringe Linearization Interferometry (FLI) for Detection of Defects". The results to date are very encouraging and show that the linear holographic fringes can be isolated on the surface of interest by swinging the object beam. The holographic image exhibits a strong first order in the Fourier Transform plan when noise is present. A filtered image demonstrating the FLI technique for a simulated defect in a triple exposure hologram has been obtained. The deformation analysis for simple models has shown agreement with experiment.

In this report we first define the research objectives and delineate the significant accomplishments to date. We then discuss the linear fringes including the use of localization techniques and the design of the experimental arrangement. The use of the apparatus for creating differential stresses with static forces and the design of the spatial filtering system are given. A simulation experiment designed to show the enhancement of defect location utilizing the holographic FLI technique is discussed. Finally, the simple static model and its agreement with experimental results is presented. The results of the study to date are described. Plans for work to be performed in Phase II are also outlined.

CONTRIBUTORS TO THE REPORT

The principal investigator of this study is George O. Reynolds from the Honeywell Electro-Optics Division. Donald A. Servaes from Honeywell is the Project Experimentalist. John B. DeVelis, a consultant to Honeywell from Merrimack College, has contributed to the holographic portion of the study. Ronald A. Mayville, Peter D. Hilton and Daniel C. Peirce from Arthur D. Little, Inc. performed mechanical designs and system analysis under a subcontract. Joseph A. Russo from Arthur D. Little has assisted with the mechanical configurations and controls.

SECTION 2
RESEARCH OBJECTIVE

The objective of the research in this program is to prove the concept of Holographic Fringe Linearization Interferometry (FLI) and determine its degree of utility. In the FLI technique, linear fringes are introduced in the formation step of double exposure holographic interferometry by utilizing a beam deflector in the object beam between the two holographic exposures. A subsequent spatial filtering operation is performed on the reconstructed image from the double exposure hologram. The filter is tuned to the frequency of the linear fringes. The purpose of the filter is to remove from the image the random noise fringes which commonly appear in double exposure holographic interferometry. These noise fringes occur due to the differential vibrations which exist in the test subject at the two different exposure times. The noise fringes are the prime cause of the difficulty in data interpretation of normal double exposure holographic interferograms. The filtering step should remove the noise fringes and enhance the presence of shifts in the linear fringes due to subsurface defects. This enhancement is expected to simplify the process of locating the defects.

The prime goal of this research program is the experimental demonstration of the FLI technique for detecting and locating (not necessarily identifying or classifying) subsurface cracks and defects in various structures. Since FLI is a large area inspection technique which is very compatible with image processing, its success can ultimately simplify the Nondestructive Evaluation (NDE) process for large military structures such as aircraft.

The initial experiments on this program were performed by Honeywell EOD at the Advanced Concepts group's optical lab in Brighton, MA. Subsequent experiments in Phase II will be performed on the NADC holographic system in Warminster, PA.

SECTION 3
PROGRESS, PRELIMINARY RESULTS AND PLANS

The program is scheduled to be a three-phase study over a three year period of time. This report discusses the work performed and the results obtained during Phase I.

The results to date indicate that the linear fringes can be placed on the surface of interest by utilizing beam swinging techniques between holographic exposures. The filtering step to remove random noise, which should enhance the ability of an observer to detect and locate a defect, has been experimentally demonstrated with simulated defects and simulated linear noise fringes which were oriented at a different angle than the linear FLI fringes in a triple exposure hologram. These results illustrate that the FLI technique is very promising. It has been determined that thermal loading and static mechanical loading can be used to create repeatable and reliable out-of-plane static stresses with our test fixtures.

In addition, we have obtained good agreement in counting fringes between a simple bending model and experiments performed by hanging weights on the test plate between holographic exposure.

In Phase II, we will transfer the experimental procedure to the holographic system in NADC in Warminster, PA, and perform both static and dynamic loading experiments aimed at locating subsurface cracks in controlled test samples. In addition, the deformation analysis will continue in order that we may better understand the mechanisms causing the fringe patterns in holographic interferometry. This fundamental understanding will help quantify our results later in the program.

SECTION 4
TECHNICAL STATUS OF RESEARCH EFFORT

4.1 THEORETICAL CONSIDERATION OF LINEAR FRINGES

4.1.1 Creation of Linear Fringes

In Appendix I, we show that an angular shift of the object beam in a double exposure Fourier transform hologram leads to linear fringes in the image reconstructed from the hologram. A similar analysis was done by Smith[1]. In Appendix II, we show that a similar effect exists in a sideband Fresnel hologram[2]. This means that linear fringes can be produced in the NADC system. However, the location of these fringes within the reconstructed image volume of a sideband Fresnel hologram depends on the geometry of the beam-shifting arrangement. Maximum contrast fringes on the object surface (fringe localization) are realized by rotating the object beam by an angle, $\delta\theta$, about either the x or y axes of the object, as discussed in Reference 3. This was accomplished in our experiments by moving the point source of a collimated object beam. If the beam shifting is accomplished by rotating the mirror in a spherical wave, then the fringes will have maximum contrast at a position in the volume other than the object surface. Preliminary experimentation indicates that the linear fringes produced with a spherical object wave can be localized on the object surface by moving the mirror in such a way that the apparent source position rotates about an axis in the object. This localization is discussed below.

4.1.2 Localization of Holographic Fringes

Fringe linearization interferometry can be easily visualized by means of the following "Gedanken" experiment. Consider a test specimen that is simultaneously in two states, one stressed and one unstressed. Further, consider that two mutually coherent point sources are used to illuminate the

specimen. One illuminates only the unstressed test specimen while the other illuminates only the stressed test specimen (i.e., a Michelson interferometer with one stressed mirror). The light from these two surfaces will interfere and the result is similar to the image from a holographic interferogram. If we further slightly displace the sources, one from the other, the result is the familiar interference pattern obtained from two displaced sources. The details of the interference pattern for the thought experiment and the holographic experiment will vary with viewing position.

The NADC holographic system incorporates a negative lens to expand the ruby laser beam so that it will illuminate the test area. This is a normal method used to obtain a spherical wavefront. This is also the method we planned for our simulation experiment. We planned to obtain the linear fringe by slightly tipping the beam angle between exposures. However, when spherical waves were used, the expected linear fringe pattern was found to exhibit a frequency change and a slight curvature as a function of field position. As shown in Appendix III, the few percent change in fringe frequency and fringe curvature should not exceed the spatial frequency bandwidth of our spatial filtering system and, ultimately, should not affect our results.

In addition, the problem of localizing the nearly linear fringes to the test surface is difficult when spherical waves are used. Vest[3] addresses this problem. He points out that, if the test specimen is rotated between successive exposures about an axis through the specimen front surface, then the holographic interferometer fringes will be localized on the surface of the specimen. This is equivalent to rotating the source along an arc whose center of rotation is on the front surface of the test specimen. This condition can be approximated (when the source is a focused laser beam spot) by the appropriate rotation of a mirror about some other center, as suggested in Figure 4-1.

Our experiments and analysis indicated that linear fringes can always be localized on the surface with plane wave illumination. Therefore, most of the simulation experiments were done with plane waves to avoid the problems associated with spherical waves. In addition, use of a plane wave reference beam yields both real and virtual images having unit magnification.

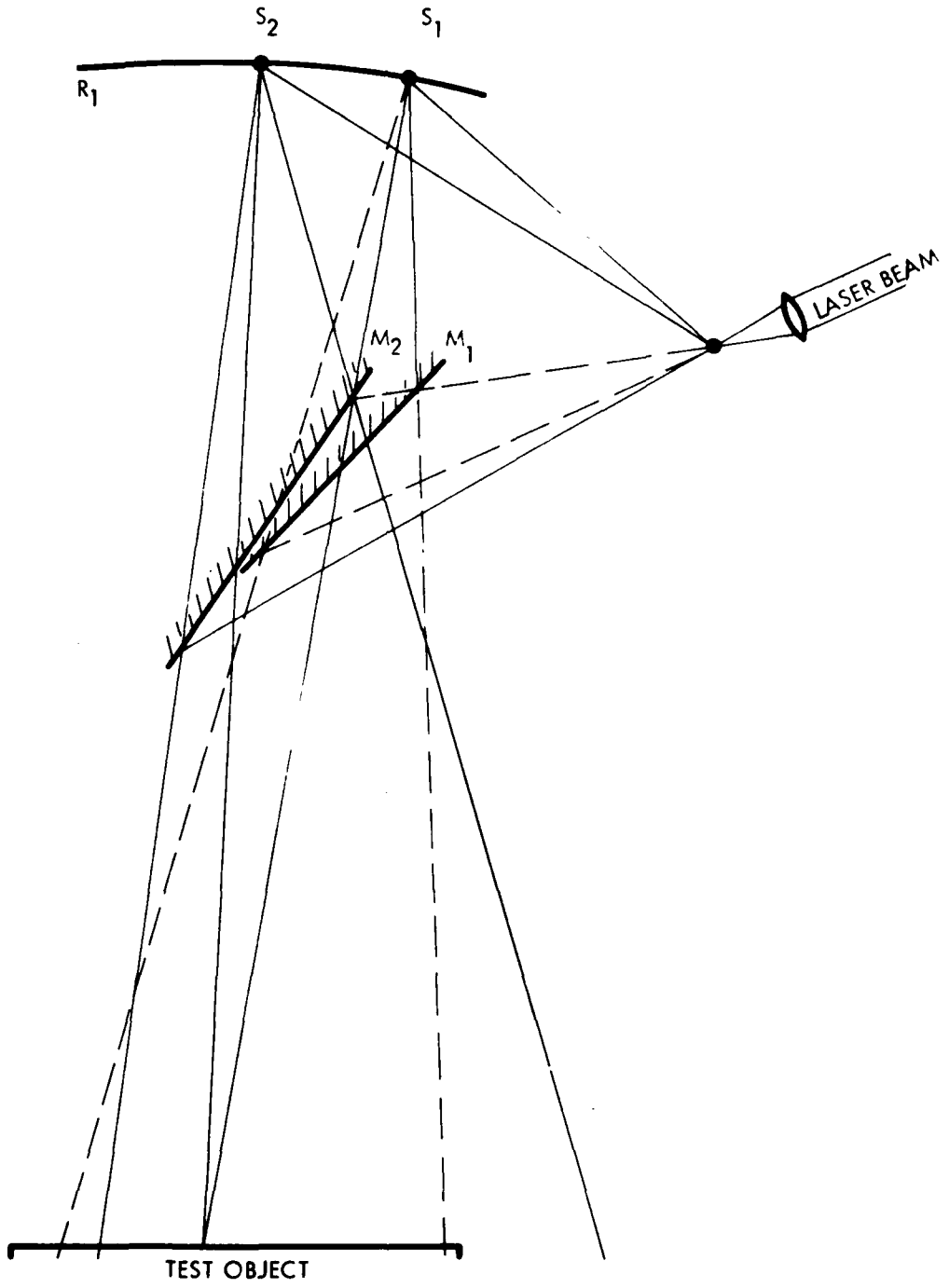

Figure 4-1. Schematic Illustrating Proposed Mirror Location

4.1.3 Illustration of Problems with Spherical Wave FLI

In order to illustrate the spherical wave problems, Figure 4-2 shows the resulting virtual image obtained from a triple exposure hologram made with spherical waves. The test specimen was stressed between the first and second exposures and the spherical wave illumination source was slightly displaced between the second and third exposures. This image illustrates that the fringes are localized on the surface, that the fringes exhibit a slight curvature across the field of the image due to the spherical waves, and that a frequency shift results. The difficulties associated with fringe localization and the problems of fringe frequency shifting and fringe curvature caused us to abandon the use of spherical wave illumination, and plane wave illumination was used in most of the experiments in Phase I. The use of spherical waves will be reconsidered in the full field experiments at NADC planned later in this program.

4.2 DESIGN OF EXPERIMENTAL FLI SYSTEM

The initial experiments performed at the EOD Optical Laboratories were planned to show that linear fringes could be observed in the reconstructed image from a double exposure holographic interferogram if the object beam was shifted between the two exposures. In addition, the enhancement of defects by spatial filtering of the reconstructed image to remove the random fringe noise was also planned as a demonstration experiment.

The experimental system chosen to demonstrate these effects was a scaled-down version of the NADC holographic system. This system was chosen so that experimentation can be shifted to the NADC system later in the program with minimal changes.

The key parameters of the NADC system which were utilized in the design of the holographic setup at EOD were:

- a 45° angle between object and reference beams, which creates a 1200 c/mm carrier frequency,

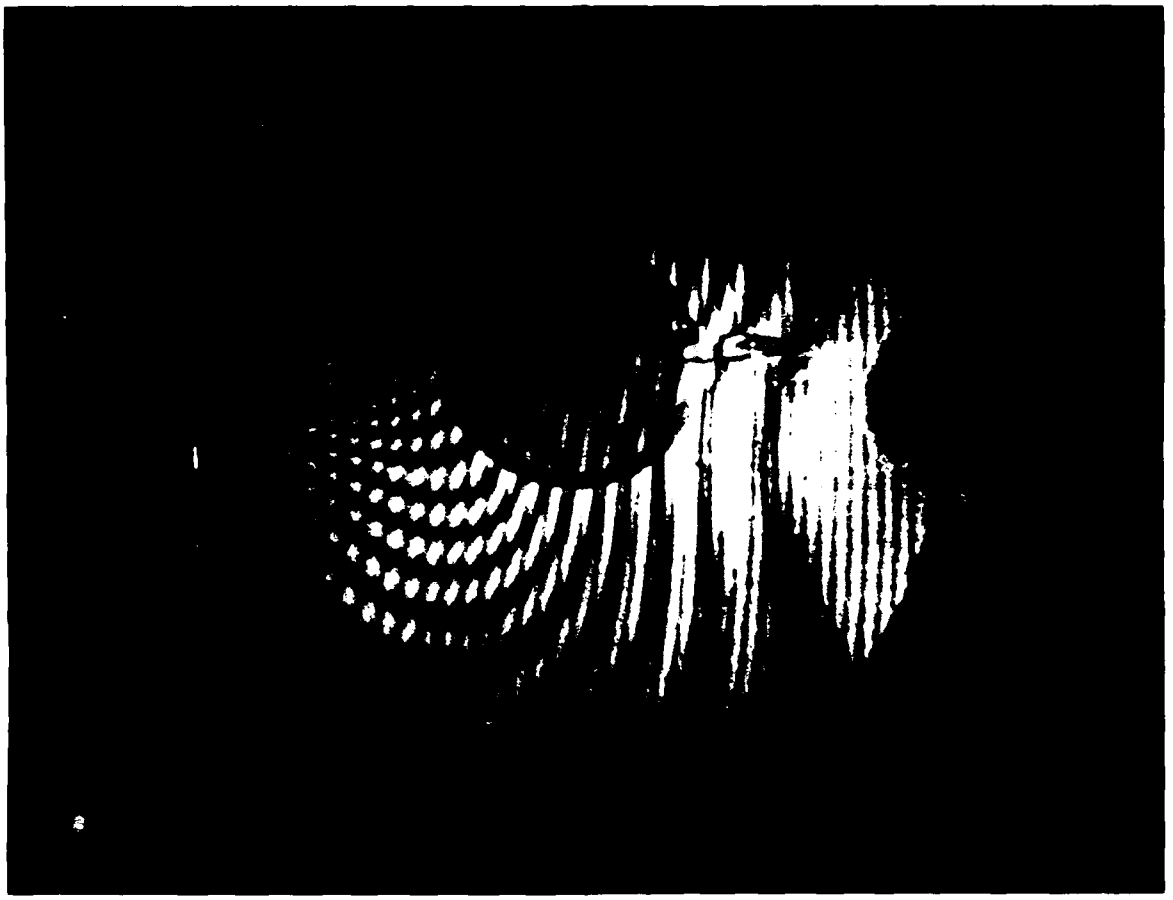

83218

Figure 4-2. Reconstructed Image Resulting from Triple Exposure Hologram Illustrating Glue Near the Crack (to the Right of Circular Plug) and the Random Noise Fringes on the Left

- Agfa Gavert 8E75HD film which is red sensitive and capable of resolving the 1200 c/mm carrier frequency,

- a three to one energy ratio between reference and object beams at the film plane to optimize diffraction efficiency, and

- a spatial filter in the laser condenser to create a nearly uniform wavefront for constructing the holograms.

A schematic diagram of this experimental arrangement is shown in Figure 4-3.

Prime differences between this experimental arrangement and the NADC system are:

- low power He-Ne CW laser (6328 Å) rather than Pulsed Ruby Laser (6943 Å)

- 1-5 s exposure times rather than the 10-100 ns exposure times of the NADC ruby laser

- a field of view of 10 cm rather than 1 meter

- movable mirror in object beam to create linear fringes

- collimated object beam to allow localization of linear fringes onto the object surface

- collimated reference beam to give unit magnification

These differences in the lab system should be readily adaptable to the NADC system. These adaptations will ensure that high-contrast, localized, linear fringes exist in the object plane of the NADC system.

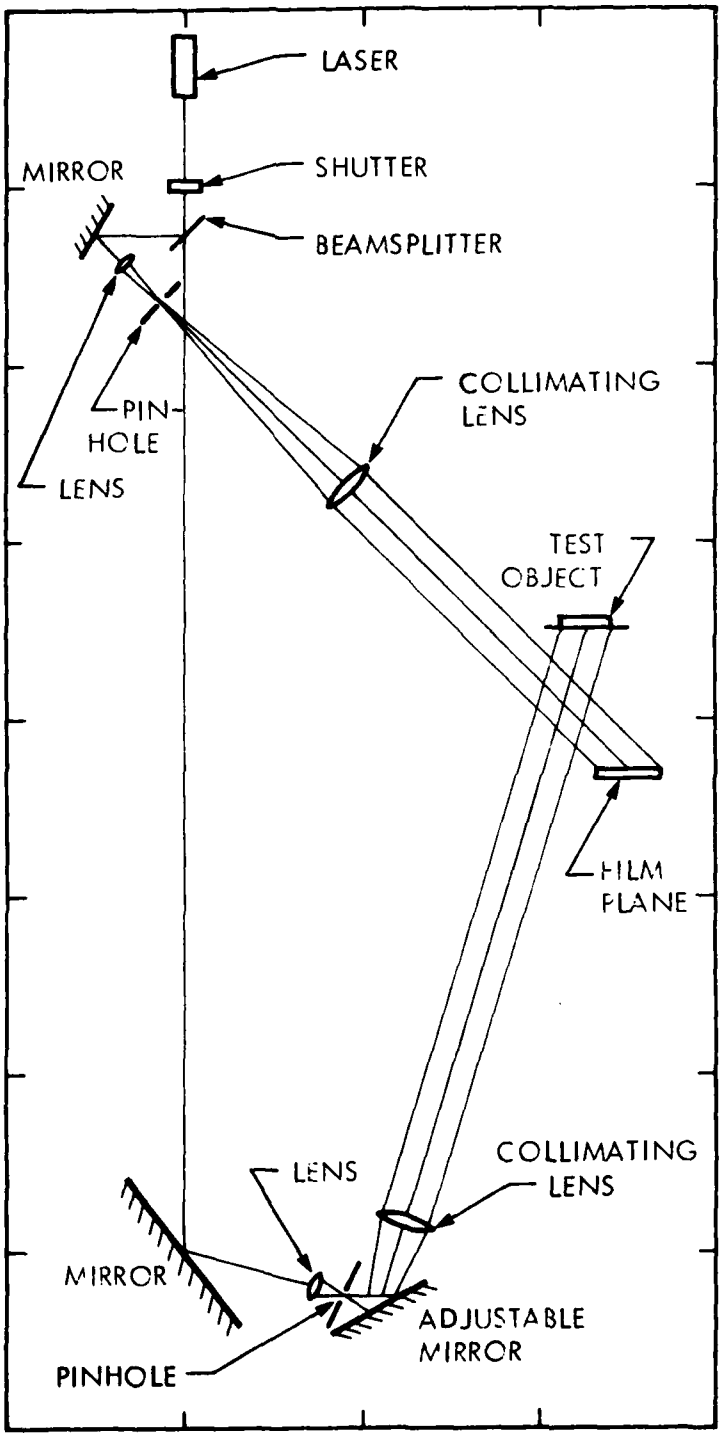

Figure 4-3. Experimental Arrangement for Holographic FLI Experiments

4.3 LINEAR FRINGES IN THE FLI SYSTEM

The NADC system was used to estimate the linear fringe frequency requirements. This linear fringe frequency was then used in the laboratory experiments at EOD.

The hologram created in the NADC system is a sideband Fresnel hologram with a 1200 c/mm carrier. Use of Equation 5-49 of Reference 2 shows that the resolution cutoff is 1227 c/mm, when it is assumed that:

film size = 3 in. = 76 mm,
carrier frequency = $\sin \alpha/\lambda$ = 1200 c/mm,
wavelength = 6.943×10^{-4} mm, (ruby laser), and
object distance = 2000 mm.

This means that 27 c/mm is available to resolve the object detail in the NADC system when a three inch diameter film is used to record the hologram. A resolution of 27 c/mm at a distance of 2 meters corresponds to an angular resolution of 54 c/mr. The angular resolution of the human eye (10 c/mm at 25 cm) is 2.5 c/mr. Thus, the NADC hologram with a three-inch film has approximately twenty times more object resolution than the human eye.

If we assume that the minimum defect width needed to be resolved by the hologram is 0.1 mm, then the spatial frequency requirement of the system is an object resolution of 5 c/mm or 10 c/mr at a distance of 2 m. This is approximately four times better than the human eye. If we further assume that our linear fringes are perpendicular to the crack, then, the number of sampling fringes per length of crack varies for different crack lengths and fringe frequencies, as shown in Table 4-1. Fringes of these frequencies requre tilt angles in the object beam between 0.35 to 17.5 mr.

Table 4-1. NUMBER OF FRINGES ALONG VARIOUS CRACK LENGTHS FOR TWO DIFFERENT LINEAR FRINGE FREQUENCIES

Crack Length (mm)	No. of Linear Fringes of Frequency 0.5 c/mm	No. of Linear Fringes of Frequency 5 c/mm	No. of Linear Fringes of Frequency 25 c/mm
1.0	0.5	5.0	25.0
0.5	0.25	2.5	12.5
2.0	1.0	10.0	50.0
3.0	1.5	15.0	75.0
4.0	2.0	20.0	100.0

4.4 CONSIDERATIONS FOR FILTERING OF THE FLI HOLOGRAMS

4.4.1 Need for Intermediate Photograph

Initial experimentation showed that it is not possible to perform spatial filtering directly in the reconstruction step of the holographic process because the transform plane, which is the image of the laser source, does not exist when the hologram is made in reflection. The reason for this is that the real world objects of interest have rough surfaces which behave as random diffusers to the laser beam. This scattering property of the object, which allows for redundancy in the hologram and parallax in the reconstructed image, also ensures the absence of a Fourier filter plane. This means that an intermediate recording of the reconstructed image will be necessary to filter the FLI holograms. In a positive vein, this removes the energy restriction which was anticipated in the filtering step because an auxillary source can be used in the filtering system. Also, the linear fringe frequency can be increased by demagnifying the image. It will also be possible to use incoherent lamps as filtering sources which reduce speckle noise in the filtered image[4].

4.4.2 Linear Processing of Intermediate Photograph

The intermediate photograph is a record of the intensity distribution in x and y of the reconstructed hologram. A lens is used to image the virtual image onto the film.

The intensity transmission of the intermediate photograph is

$$T(x,y) = 10^{-D(x,y)} \quad , \qquad (4.1)$$

where D(x,y) is the photographic density distribution of the film.

The spatial filtering is done in a coherent optical system, which is an amplitude transmission system. Intensity is defined as the square of the amplitude, or, more exactly, $I = AA^*$. Therefore, $A = \sqrt{I}$ and the amplitude transmission of the photograph is

$$T_A(x,y) = 10^{-D(x,y)/2} \quad . \qquad (4.2)$$

The film density, D(x,y), is given by

$$D(x,y) = \gamma \log I(x,y)t = \gamma \log I(x,y) + \gamma \log t, \qquad (4.3)$$

where gamma (γ) is the slope of the H & D curve of the photographic process and t represents the exposure time.

Equation (4.3) can be written

$$D(x,y) = \gamma \log I(x,y) + C \qquad (4.4)$$

where C is the constant $\gamma \log t = \log t^{\gamma}$.

The amplitude transmission is given by combining Equations (4.2) and (4.4), i.e.,

$$T_A(x,y) = 10^{-D/2} = K10^{-(1/2)\log I^{\gamma}(x,y)} \qquad (4.5)$$

where K is the constant t^{γ}.

Equation 4.5 can be more simply written as

$$T_A(x,y) = I^{-\gamma/2}(x,y). \qquad (4.6)$$

Equation (4.6) relates the amplitude transmission of the film to the intensity distribution in the photographic image. The condition of *linearity processing* is given by

$$\gamma = -2 \cdot \tag{4.7}$$

Various discussions of linear processing and recipes for realizing this condition have appeared in the literature[5,6,7].

Equation (4.7) means that the film must be processed as a positive. The amount of tolerance from linear processing allowable on the photographic process in the FLI technique will have to be determined experimentally. Our early experience on other experiments shows that a tolerance of a few per cent is usually acceptable.

4.4.3 Additional Constraints

An additional constraint that the filtering step imposes on the FLI system concerns the frequency of the linear fringes. The fringe frequency must be great enough to realize a separation of a few millimeters between the diffraction orders in the transform plane. This requirement is necessary to: (1) avoid aliasing in the filtered image, (2) have a fringe contrast greater than 50% or 60% on the intermediate photograph, and (3) create a reasonable working region in the transform plane which eases the filter fabrication problems. For the 10 inch focal length lens used in our experiments, we found that fringe frequencies of 25 c/mm gave separations between 3 and 4 mm, which was reasonable. It is also possible to double this separation by using spherical wave illumination in the filtering system[8].

4.5 ANALYSIS FOR SPATIAL FILTERING OF FLI GENERATED IMAGES

This section will illustrate the advantage of the holographic FLI technique over conventional double pulsed holography in detecting defects in the presence of fringe noise.

Equation (I.4) of Appendix I illustrates that the reconstructed image in FLI is laced with linear fringes having a spatial frequency proportional to the angular shift, $\delta\theta$, introduced between the two object beams. Note: In going from Equation (I.3) to Equation (I.4) in Appendix I, we assumed that $f(x',t) = f(x', t_1)$, i.e., no differential disturbance exists between the two exposures.

4.5.1 Response of the Defect

In order to extend this analysis to include the response of the defect to mechanical impulses, assume that the defect of interest causes a differential surface stress, $\Delta\phi(x')$, (due to an impulse) between the two exposures. Deformations caused by this stress behave as an optical phase function in the hologram. Then a simplified analysis would assume

$$f(x', t) = 1 \quad ,$$

and

$$f(x', t_1) = \exp[ik\Delta\phi(x')] \quad ,$$

in Equation (I.3) of Appendix I.

Under these conditions, the revised image of Equation (I.4) in Appendix I would be

$$\text{ideal image} = 2 + 2\cos\left[\frac{kx_0x'}{f} + k\Delta\phi(x')\right] \quad , \tag{4.8}$$

i.e., the surface stress differential appears as a phase modulation of the linear fringes and has a shape, size and location, $\phi(x')$, characteristic of the defect. We call this the ideal image because of the simplifying assumptions used in deriving Equation (4.8).

An interesting example illustrating this phase modulation is the image hologram of the phase object "ϕ phase" shown in Figure 4-4.

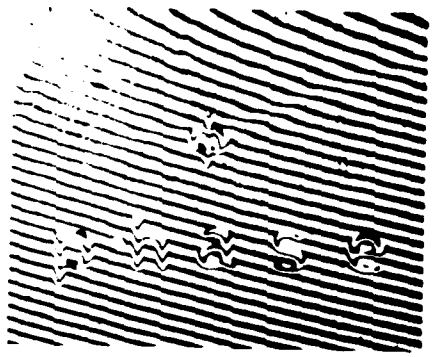

Figure 4-4. The Object (Defect) in this Experiment is the Letter "ϕ" and the Work "Phase". The Image Hologram of the Object Shows That the *Phase Modulation of the Linear Fringes* Reveals the Shape of the Phase Deformation (Defect). (From Reference 2)

This simple extension of the analysis illustrates that spatial phase distributions are indeed carried as a phase modulation on the linear fringes.

4.5.2 Removal of Random Fringe Pattern

Now, consider the random fringe pattern that is associated with double pulse holography, such as the complex fringe structure in Figure 4-5. The simple O'Neill filter will remove this random fringe pattern[9,10].

In order to show this mathematically, let

$$f(x',t_1) = F_R(x',t_1)\exp[ik\Delta\phi(x')]$$

in Equation (I.3) of Appendix I.

Figure 4-5. Complicated Fringe Pattern on a 48 by 25 Inch Panel Using the Pulsed Holographic NDT Technique. The areas of stress corrosion cracking are indicated by fringe shifts in the boxed-in areas (From Ref. 11).

This means that the random fringe displacement in a double exposure holographic interferogram (e.g., see Figure 4-5) having amplitude $F_R(x',t_1)$ is due to the change in surface stress between the first and second holographic exposures and is all coupled into the term $f(x',t_1)$ for simplicity.

With these assumptions, Equation (I.4) of Appendix I becomes

$$\text{Image} = 1 + [F_R(x',t_1)]^2 + F_R(x',t_1)\cos\left[\frac{kx_0x'}{f} + k\Delta\phi(x')\right]. \quad (4.9)$$

The image described by Equation (4.9) can be directly processed through a Fourier processing system such as the one shown in Figure 4-6.

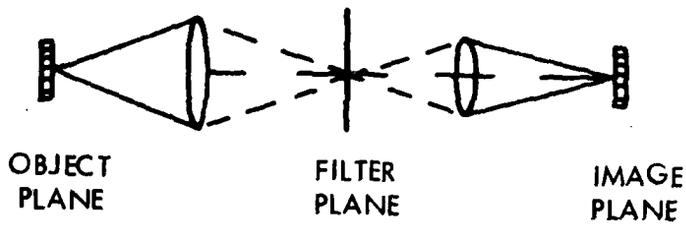

Figure 4-6. Optical Spatial Filtering System

In this processing system, the image of Equation (4.9) is Fourier transformed and passed through three pinholes in the filter plane (one located on axis and the other two at the positions of the delta functions corresponding to the linear fringe frequency). These pinholes (filters) are adjusted in size so that the frequency information, $\Delta\phi(x')$, contained in the fringe shift associated with the defects is passed, and the frequency information due to the noise, $F_R(x', t_1)$, is blocked by the spatial filter.

Upon retransformation, the filtered image will be:

$$\text{Filtered image} = 2 + 2\, M_L(x')\cos\left[\frac{kx_0x'}{f} + k\Delta\phi(x')\right] . \qquad (4.10)$$

The Amplitude Modulation, $M_L(x')$, in the filtered image represents the nonuniform intensity of the image. This modulation exists because the random fringe distribution of Figure 4-5 has some energy in its Fourier transform at the location of the pinholes. This gives rise to a nonuniform intensity in the background of the filtered image. Experimental adjustment of the pinhole sizes in the filter plane will minimize the effect of this nonuniform background.

Comparison of Equations (4.8) and (4.10) shows that, when the background variation $M_L(x')$ in Equation (4.10) is small, the output of the filter is close to the ideal image. This is the effect that we are attempting to demonstrate in our initial experiments.

A similar analysis for the sideband Fresnel hologram of Appendix II also shows that random surface displacements behave as a phase modulation to the linear fringes.

4.6 OTHER TYPES OF SPATIAL FILTERS

The intensity distribution of the Fourier transform of the linear fringe pattern alone is schematically shown in Figure 4-7.

From Equation (4.10), we would expect the Fourier spectrum of the noise fringes to be convolved about each of the diffraction spikes shown in Figure 4-7. The O'Neill filter just discussed should remove the random fringe noise.

It is anticipated that cracks will produce sharp discontinuities in the linear fringe pattern. Another possible filter to enhance the location of this defect, in addition to the O'Neill filter, would be a pair of pinholes separated by the appropriate distance to see the linear fringe frequency but placed in the high frequency segment of the filter plane.

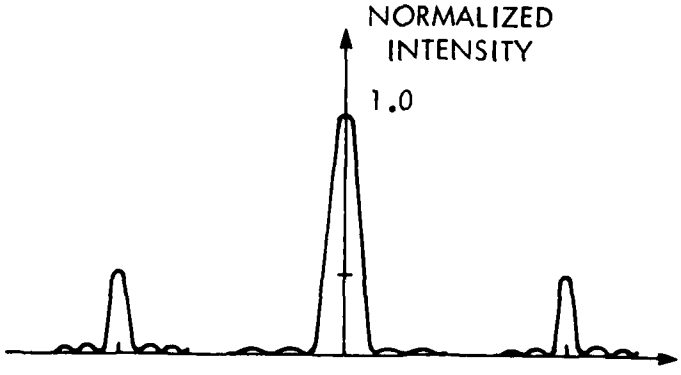

Figure 4-7. Cross-section of the Fourier Transform of the Linear Fringes

The spatial separation of the first-order component fringe spectra is given by

$$r_\rho = f_0 \lambda Z \quad , \qquad (4.11)$$

where

Z = focal length of the transform lens,
f_0 = grating frequency, and
λ = wavelength of the radiation.

If we have a 25 c/mm linear fringe frequency, a 10-inch focal length lens, and a wavelength of 6238 Å for the He-Ne laser, then we have a pinhole filter separation given by

$$r_\rho = 3.9 \text{ mm}.$$

Clearly, this separation will change with different fringe frequencies, focal length lenses, and system magnifications.

Another possible filter would pass the desired object information in the filter plane and not pass the higher frequency speckle noise (i.e., a low pass filter). An off-axis iris stop could be used in the transform plane to achieve this effect. Still another filter could be an annular ring tuned to the spatial frequencies of the phase shift caused by the defect. Various spatial filters will be investigated during the remainder of this study.

4.7 DESIGN CONSIDERATIONS FOR TEST SPECIMEN AND FIXTURE FOR PERFORMING HOLOGRAPHIC FLI WITH STATIC FORCES

The purpose of the test specimen and fixture is to provide a configuration in which geometry and deformations can be controlled for the study of the application of fringe linearization to holographic interferometry. Our particular objective is to use the test specimen and fixture to establish the capability and sensitivity of the holographic technique to detect cracks and crack-like defects.

There are several requirements for the test apparatus. Its primary function is to induce some form of deformation between hologram formations so that linear fringe shifts can be constructed. The deformation pattern must result in a gradient of out-of-plane displacements which is large enough to cause a series of shifts but which is not too large to make the fringes indistinguishable. Because we wish to study the sensitivity of our holographic technique, the apparatus must also provide interchangeability for specimens containing cracks of different shapes and sizes. In another phase of this investigation, we will use analytic techniques to calculate the deformations characteristic of certain crack sizes and shapes. This will be done for the purpose of studying the sensitivity of the fringe linearization method without using specimens and to compare calculated, constant, out-of-plane displacement contours to interferometric fringe patterns. Therefore, it is necessary to know the boundary conditions for the test specimen with some accuracy so that analytic predictions can be made.

Several different test configurations have been used to investigate the detection of flaws with holographic interferometry. Vest, McKague and Friesem[12] investigated several methods but obtained the best results with a configuration in which a bolt with a tapered shank was forced into a hole between hologram constructions. Other methods that have been successful are the use of thermally induced stresses and deformations[13], and the application of a differential pressure to a thin plate acting as a membrane[14].

Each of the test configurations described above has the common feature that the boundaries of the specimen are fixed, which prohibits rigid body displacements.

All of the methods incorporate interchangeability, but it is very difficult to determine what the applied stresses or displacements are; that is, the boundary conditions are unknown.

4.7.1 Concept

In our test apparatus, we employ the interference fit concept used by Vest, McKague and Friesem. Instead of using a mechanical method to insert a bolt into the hole, we use thermal contraction and expansion.

The test specimen is a rectangular, aluminum plate with a circular hole located at its center. The plate is clamped on any one or all three of its sides in a fixture which is fixed to the optical table. A steel, cylindrical plug whose diameter is slightly larger than the diameter of the hole in the plate is submerged in liquid nitrogen, which causes the plug diameter to decrease enough to be easily inserted into the hole. The plug is inserted into the hole after the first hologram is recorded. When the plug reaches room temperature, which results in pressure on the inside of the hole, the second hologram is made.

The stresses and deformations resulting from an interference fit of this type can be approximated by using a solution from the theory of elasticity for the shrink-fitting of cylinders. For the shrink fitting of a solid cylinder in a cylindrical hole in an infinite medium, the solid cylinder having a diameter which exceeds that of the hole by an amount δ, the pressure at the interface is[15]

$$P = \frac{\delta}{D}\left[\frac{1 - V_1}{E_1} + \frac{1 + V_2}{E_2}\right]^{-1}, \qquad (4.12)$$

where

D = the diameter of the cylinder and hole after shrink fitting,
E_1, V_1 = Young's modulus and Poisson's ratio for the cylinder material,
E_2, V_2 = Young's modulus and Poisson's ratio for the plate material.

For example, for steel,

$$E_1 = 210 \times 10^3 \text{ n Pa } (30 \times 10^6 \text{ psi}) \; ; \; V_1 = 0.28,$$

and, for aluminum,

$$E_2 = 69 \times 10^3 \text{ n Pa } (10 \times 10^6 \text{ psi}) \; ; \; V_2 = 0.34.$$

The difference, δ, cannot be arbitrary. The plug diameter must be larger than the hole diameter by only an amount which can be reduced by immersion in liquid nitrogen to create a shrink fitting. After returning to room temperature, a sufficient pressure is provided so that controlled out-of-plane displacements can be detected. The change in diameter, ΔD, corresponding to a change in temperature, ΔT, is given by

$$\Delta D = D\alpha\Delta T, \tag{4.13}$$

where α = coefficient of thermal expansion. Liquid nitrogen has a temperature of -196°C and for steel, $\alpha = 11.7 \times 10^{-6}/°C$, with D = 25 mm (1 in.).

$$\Delta D = (25)\ (11.7 \times 10^{-6})\ (20 - (-196)) = 0.0625 \text{ mm } (2.5 \times 10^{-3} \text{ in.})$$

Therefore, if we machine the plug so that its diameter is 0.0625 mm greater than the hole in the plate, theoretically, we should be able to insert the plug into the hole after immersing it in liquid nitrogen. In this case, $\delta = \Delta D$. In reality, some tolerance is required because it is impossible to insert the plug with perfect alignment. This is accomplished by using a plug which, when immersed in liquid nitrogen, has a slightly smaller diameter than the hole in the plate ($\delta < \Delta D$).

4.7.2 Test Specimen and Fixture Description

The test specimen designed for the FLI experiments is a 100 mm x 100 mm x 3.125 mm (4 in. x 4 in. x 0.125 in.) aluminum plate which has a circular hole located at its center. The diameter of the hole is 24.94 mm (0.9976 in.). The steel plug that is used for the interference fit is made of leaded steel to enhance the surface finish and maintain tolerances on the shank diameter which is 24.98 mm (0.9992 in.). The shank length is 2.5 mm (0.100 in.). The end ischamfered to facilitate insertion, and the other end has a

shoulder to ensure alignment. The difference in diameter is δ = 0.04 mm (1.6 x 10^{-3} in.) which is less than the amount of contraction which occurs when the plug is immersed in liquid nitrogen (0.0625 mm or 2.5 x 10^{-3} in.). This provides a sufficient tolerance to easily insert the plug into the hole. After the plug is inserted, one must hold the plug until enough expansion has occurred for it to retain itself; this takes about one minute. The entire system returns to room temperature in about 10-15 minutes. Schematic drawings of the specimen, without a crack, and the plug are shown in Figures 4-8 and 4-9.

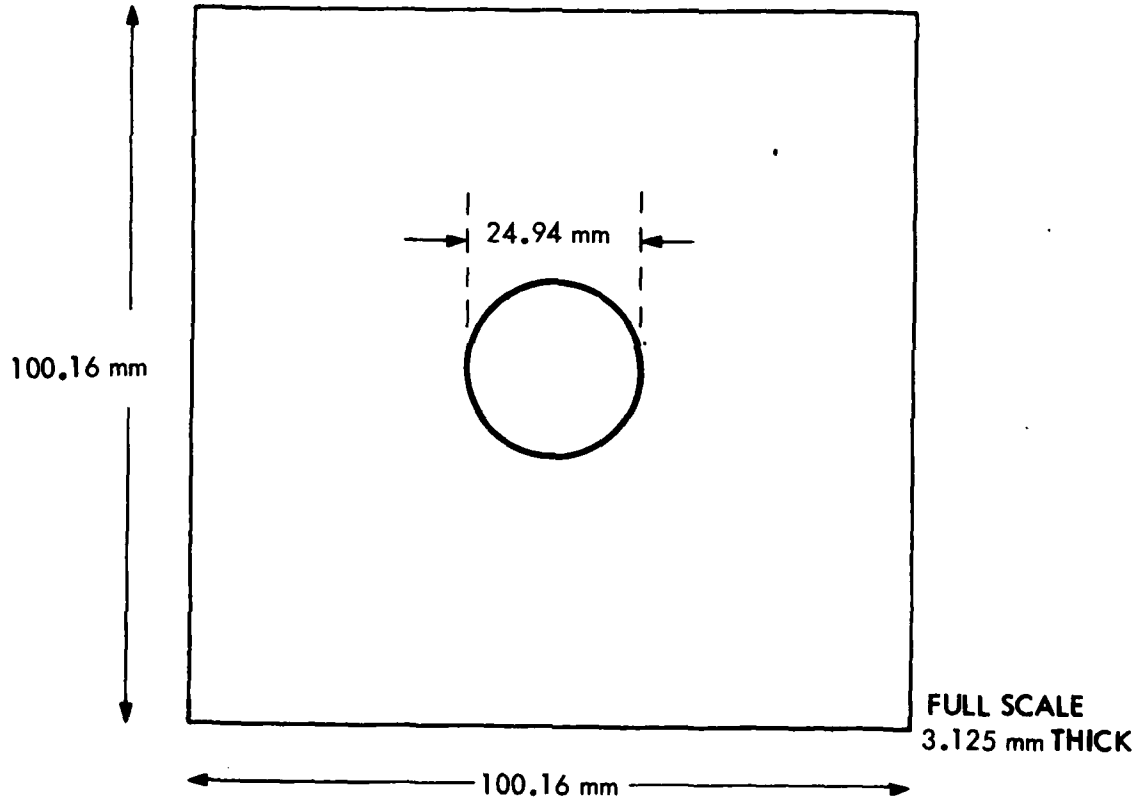

Figure 4-8. Aluminum Test Specimen Geometry

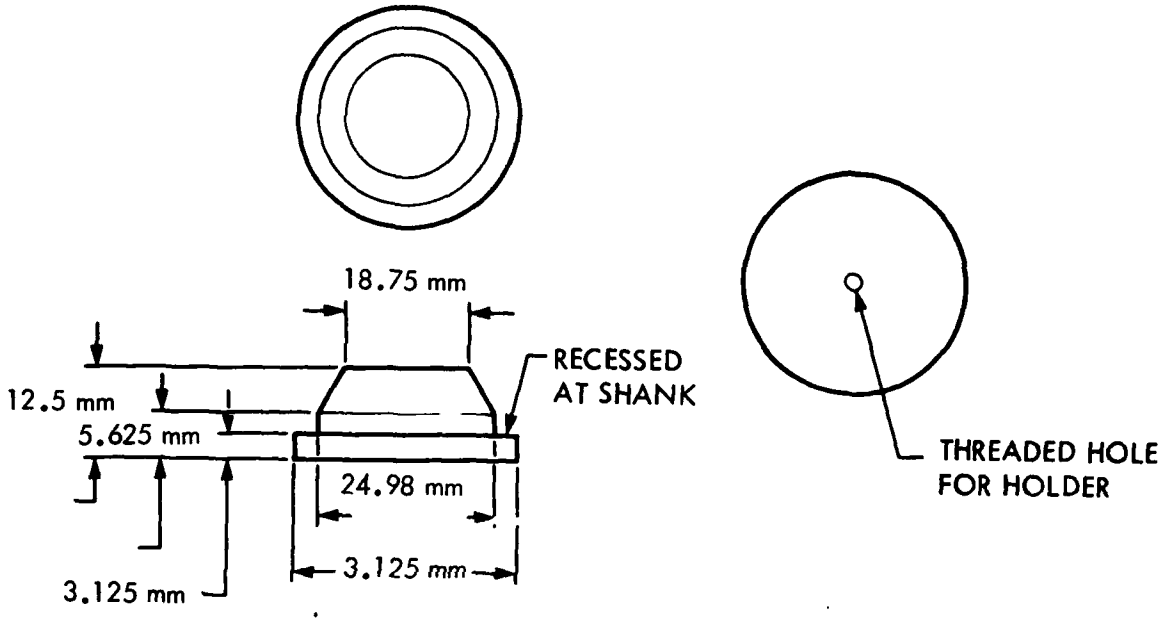

Figure 4-9. Steel Plug Geometry

A sketch of the fixture is shown in Figure 4-10. It is made of aluminum with holes in the base for attachment to the optical table. The sides of the fixture are designed to be very stiff to accommodate an anticipated experiment in which a load is applied perpendicular to the plate to obtain direct out-of-plane displacements as in the membrane method. The specimen can be held by three clamping bars - one on each side and one on the bottom - which are set by two thumb screws each. The specimen is inserted and clamped prior to constructing the holograms. The fixture is designed so that the specimen is easily removed. In actuality, many different test pieces will be utilized during this program.

After the plug has been inserted in the specimen and both holograms have been made, the plug must be removed. This is accomplished by removing the specimen and plug and placing these two on a hot plate. The two pieces are heated until the steel plug can be easily removed. This can be done because the aluminum has a coefficient of thermal expansion twice that of steel.

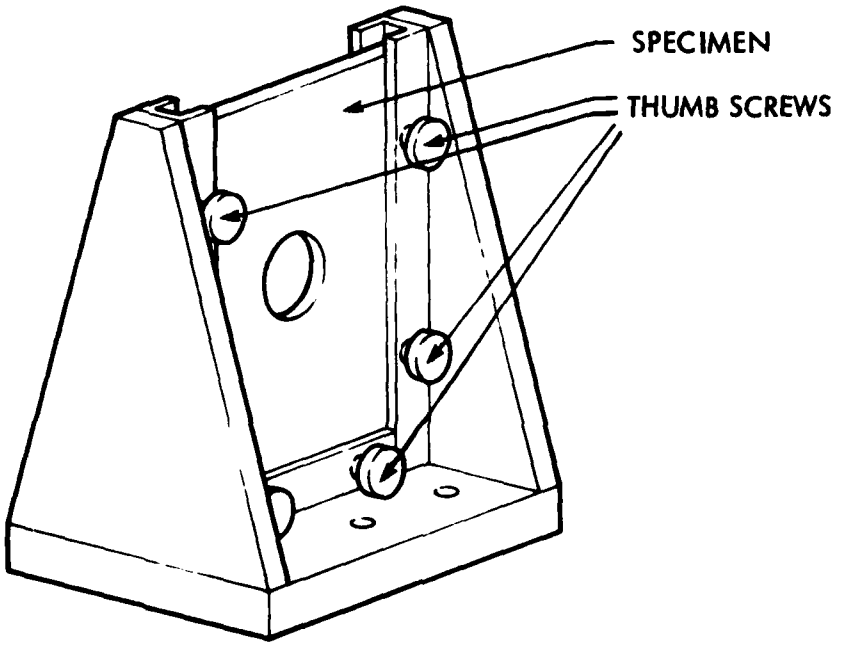

Figure 4-10. Sketch of the Test Fixture With Specimen.

4.8 A SIMULATION EXPERIMENT USING TEST SPECIMEN TO DEMONSTRATE FILTERING OF RANDOM NOISE FRINGES FROM FLI HOLOGRAMS

4.8.1 Initial Experiment

A simulation experiment utilizing stresses arising from static forces was designed to demonstrate the filtering step of the holographic FLI technique. In this experiment, the test specimen having the cut in the plate (through crack) emanating radially from the hole was used. A thin layer of glue was placed over the cut in one of the holographic exposures to enhance the expected out-of-plane motion of the crack. This glue behaves as a simulated defect. Random fringe noise of the type anticipated in the dynamic loading experiments was introduced with an additional holographic exposure. The

simulated hologram was made by using separate holographic exposures with spherical waves, as described below:

1st Exposure - A hologram was made of the specimen having a layer of glue over the crack and thermally stressed by the cold plug returning to room temperature.

2nd Holographic Exposure - The specimen was then loosened in its fixture by unscrewing one of the six support bolts. This creates large out-of-plane motions on the specimen near the loose bolt. This motion simulates random noise fringes in the reconstructed image of the type usually observed with dynamically loaded double-exposure holographic interferometry (e.g., see Figure 4-5). These are the fringes which should be removed by the spatial filter.

3rd Holographic Exposure - The glue is removed from over the crack and the object beam tilted to introduce the linear fringes (ω_o-5 c/mm) before this exposure is made.

The first and third exposures comprise the normal FLI system, with the second exposure simulating the noise. An example of the image reconstructed from this triple exposure hologram is shown in Figure 4-11. The linear fringes are clearly observed on the right. The path length changes, caused by removing the glue between exposures 1 and 3, allowing the simulated defect (oblong glob to the right of the circular plug) to be seen.

In Figure 4-11, the linear fringes are in the vertical direction with the high frequency simulated noise fringes in the horizontal direction (to the left in Figure 4-11), low frequency noise fringes at an angle of approximately 15° to the normal (across the plug), and very low frequency noise fringes (caused by loosening the bolt) in the vertical direction (to the right in Figure 4-11). Since these low-frequency noise fringes are in the same direction as the linear fringes, they are difficult to remove with spatial filtering.

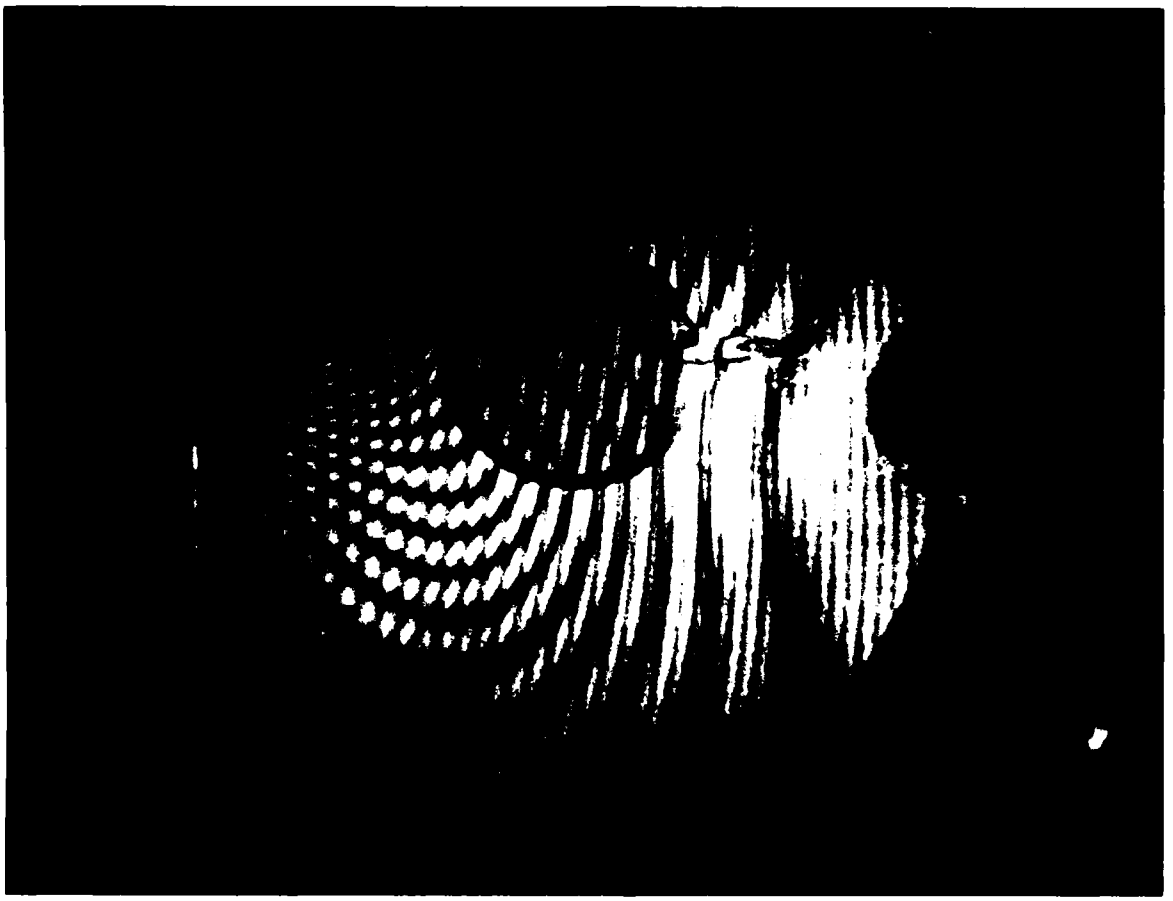

93218

Figure 4-11. Reconstructed Image Resulting From Triple Exposure Hologram Illustrating Glue Near the Crack (to the Right of Circular Plug) and the Random Noise Fringes on the Left.

A positive transparency of this image was placed in the filtering system shown in Figure 4-12. A filter consisting of three pinholes was used in the Fourier plane.

This filter was selected to pass the frequency of the linear fringes and their high-frequency fringe shifts due to the glue but to discriminate against the noise fringes which are diffracted in other directions in the transform plane.

A photograph of the distribution in the transform plane is shown in Figure 4-13. This photo shows the presence of the linear fringe frequency (middle dot on the right-hand and left-hand sides of figure) and additional spatially separable spikes due to the Moire fringes caused by the third exposure.

In this experiment, the frequency of the linear fringes was chosen to be resolvable by the human eye. This makes the filter fabrication difficult because of the small size of the light distribution in the Fourier Transform plane. The filter plane distribution at actual scale is shown in Figure 4-14.

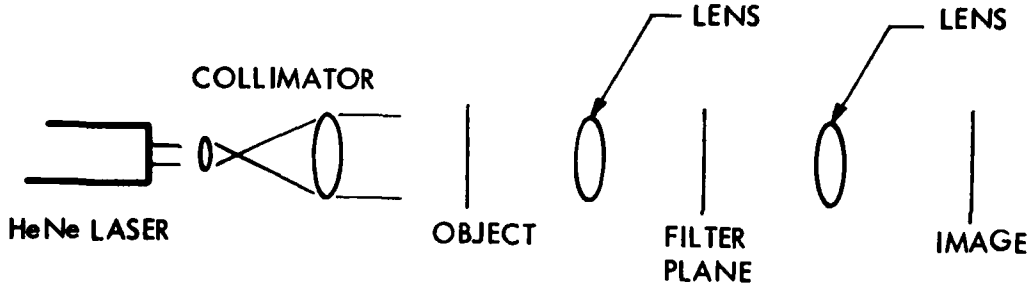

Figure 4-12. System for Filtering Doubly Exposed Simulated FLI Hologram

Figure 4-13. Transform Image From Simulated Experiment Illustrating Presence of Linear Fringe Frequency

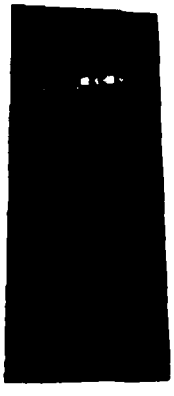

63212

Figure 4-14. Light Distribution in Transform Plane at Actual Scale

The filter for this experiment was made by punching holes in the photographic paper at the location of the linear fringe frequencies in the transform plane. The center hole limits the image resolution to very low frequencies; i.e., the edges were not sharp. The holes reject the frequency information of the crack (i.e., light in the perpendicular direction). We were able to double the filter plane size by illuminating the object of the filter system with diverging light, which located the filter plane at the second transform lens while maintaining a 1x image. However, the filter plane distribution was still too small to appreciably vary the filter geometry from the small pinholes.

The results of the low-frequency linear fringe filtering experiment (with pinhole filters) are shown in Figure 4-15. Some of the noise is rejected because the filter is programmed to pass the linear fringes. However, this filter also rejects the information concerning the simulated defect, and, hence, the defect is not emphasized in the filtered image.

This experiment was very important for a number of reasons:

1. It showed that we could localize the linear fringes with spherical waves, although with great experimental difficulty.

2. It demonstrated that spherical wave illumination placed a slight curvature on the linear fringes, as explained in Appendix III and Section 4.1.

3. It demonstrated that a small frequency variation of the linear fringes existed across the field when spherical waves were used.

4. It illustrated the difficulty of fabricating filters and their inability to pass sufficient object information when low-frequency linear fringes (5 c/mm) are used.

5. It illustrated that filtering is possible when photographic gammas not equal to minus two (-2) were used.

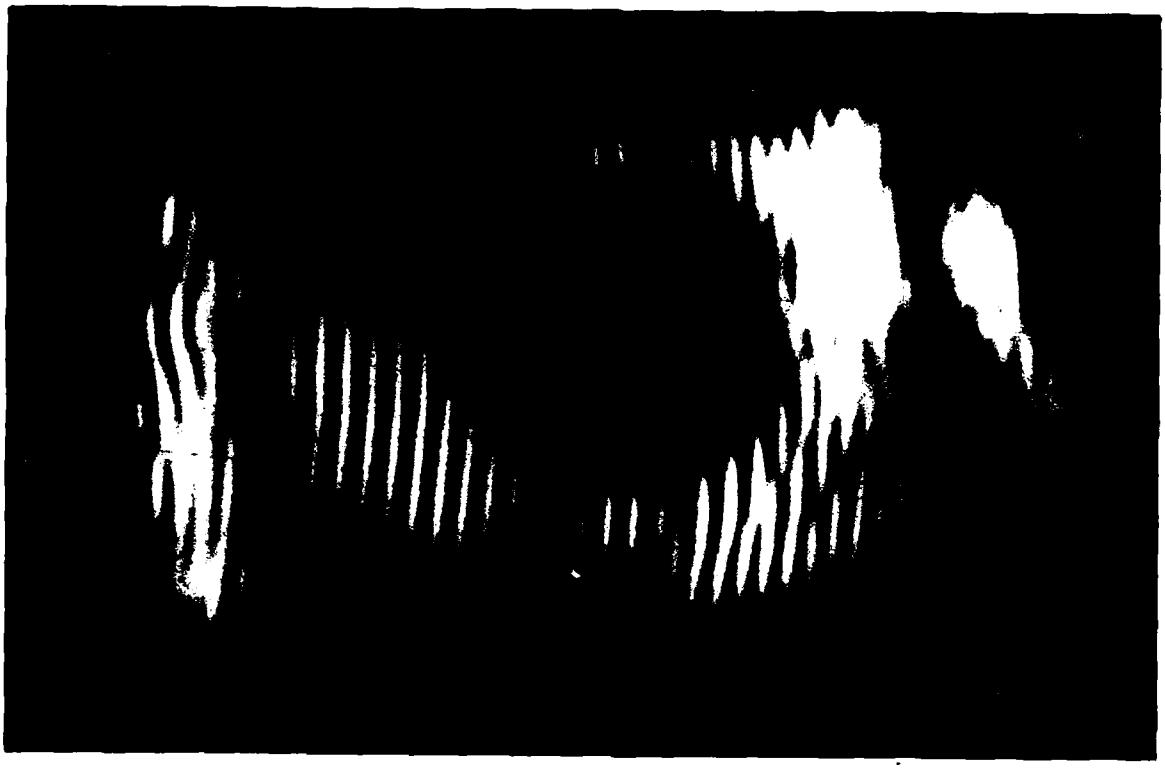

83211

Figure 4-15. Output Image Through Three-Pinhole Filter Which is Tuned to the Linear Fringes

Even with these difficulties, we showed that the noise fringes could be removed. However, the resulting image has low resolution, due to the small pinholes in the filter, and linear fringes that have a ropey appearance, due to the phase deformations caused by the spherical waves in the experiment.

4.8.2 Design of Second Experiment

In order to overcome these difficulties, the following changes were made in the experimental system:

a. Collimating lenses were used to create plane waves. These plane waves made the fringes easy to localize on the surface and eliminated the problems of fringe frequency variation and fringe curvature across the field.

b. The frequency of the linear fringes was increased to approximately 25 c/mm by increasing the angle of the object beam deflection between the exposures by a factor of five. This higher fringe frequency increased the working area in the filter plane by nearly an order of magnitude, which made the filter fabrication easier and allowed the use of larger pinholes. These filters increased the information content of the filtered image.

The triple-exposure experiment was repeated with these system changes and the results obtained are described below.

4.8.3 Results of Second Simulation Experiment

In this experiment, the test specimen with the circular plug and a through crack emanating radially from the hole was used. The defect was enhanced by placing an optically transparent material (glue or plastic strips) above the crack. Fringe noise was added with an additional holographic exposure. The simulated hologram was made by using the following three separate holographic exposures:

1st Exposure - A hologram was made of the specimen with a 1-mil thick mylar strip above the crack and thermally stressed by the cold plug returning to room temperature.

2nd Exposure - The plastic strip was removed and the beam tilted to introduce linear fringes (ω_o ~25 c/mm) before making this exposure.

3rd Exposure - The specimen was linearly tipped in the 45° direction to introduce a controlled noise fringe and the 3rd holographic exposure was made.

The first and second exposures comprise the normal FLI system and the third exposure simulates the noise.

An example of the image reconstructed from this triple exposure holograph is shown in Figure 4-16. The linear fringes are observable in the vertical direction. The simulated defect (plastic) is visible above the crack and the noise fringes are seen in the 45° direction.

A positive transparency of this image was made and placed in the filtering system. A photograph of the distribution in the transform plane is shown in Figure 4-17.

The linear fringe information is along the horizontal axis and the simulated noise spectrum is located in the 45° direction above and below the horizontal axis. A simple slit filter removed the noise and yielded the result shown in Figure 4-18.

The noise fringes have clearly been removed and the large phase shift at the position of the simulated defect remains. These results illustrate that the FLI concept is experimentally feasible.

4.9 TESTING AND ANALYSIS FOR THE DETECTION OF FLAWS WITH STATIC FORCES BY HOLOGRAPHIC INTERFEROGRAMS

4.9.1 Introduction

Initial holographic experiments with the 1.6 mm (0.0625in.) thick specimen clamped on three edges in the fixture were unsuccessful in generating fringe patterns. Nevertheless, Vest, McKague and Friesem's results[12] and our own subsequent experiments with a thicker plate described below showed that fringes were generated for a plate with a circular hole loaded by internal pressure. Since this method created fringes which made the crack visible, effort has been concentrated on understanding precisely how the observed fringe pattern arises, on qualifying the fringe pattern, and on determination of the characteristics of the pressure loading which generate a fringe pattern useful for flaw detection.

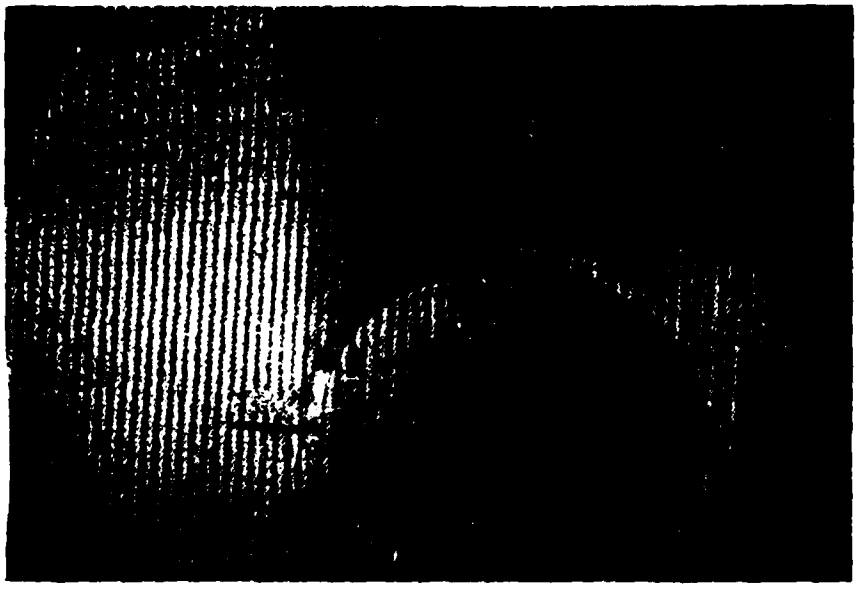

Figure 16. Reconstructed Image from Triple Exposure Hologram (Unfiltered)

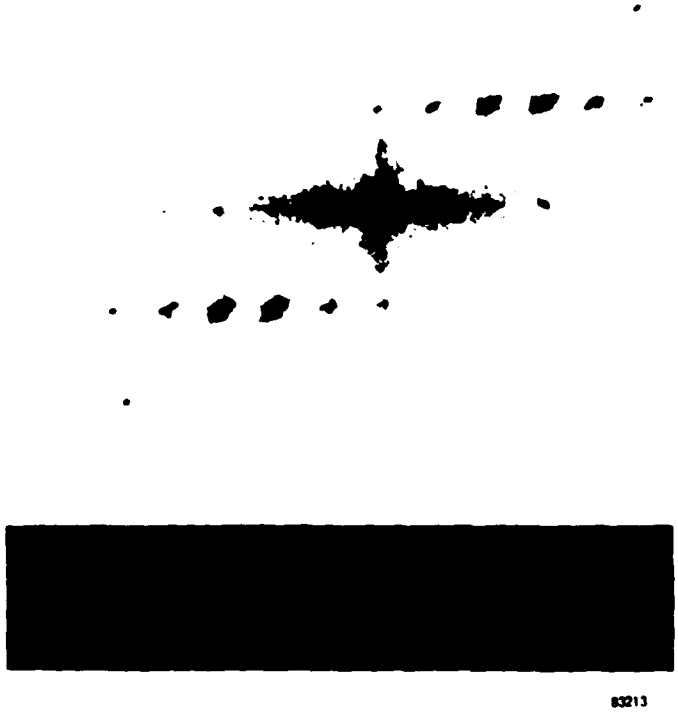

83213

Figure 4-17. Fourier Spectrum of Unfiltered Triple Exposure Holographic Image and Scale

83214

Figure 4-18. Filtered Image From Figure 1 Through a Slit Filter

4.9.2 Additional Specimen Fabrication

Three plate specimens were fabricated for these experiments. Each of these plates had a thickness of 3.2 mm (0.125 in.) with the planar dimensions reported in Section 4.7. One of the specimens did not contain a flaw but the other two did; one with a through crack and one with a part-through crack. The flaws extended from the hole at an angle of about 45 degrees to the vertical, as shown in Figure 4-19.

The flaws were machined into the plates with a small circular saw before the final 25 mm (1 in.) diameter hole was machined. For the part-through flaw, the depth of the saw cut penetrated only 80% of the plate thickness. The length of each flaw was about 25 mm (1 in.), as measured from the edge of the hole.

An attempt was made to produce a sharp crack in a 7075 aluminum plate tempered to its most susceptible condition for stress corrosion cracking by immersing the plate loaded with a tapered plug in a 3.5% NaCl solution. The method proved to be unsuccessful and was abandoned.

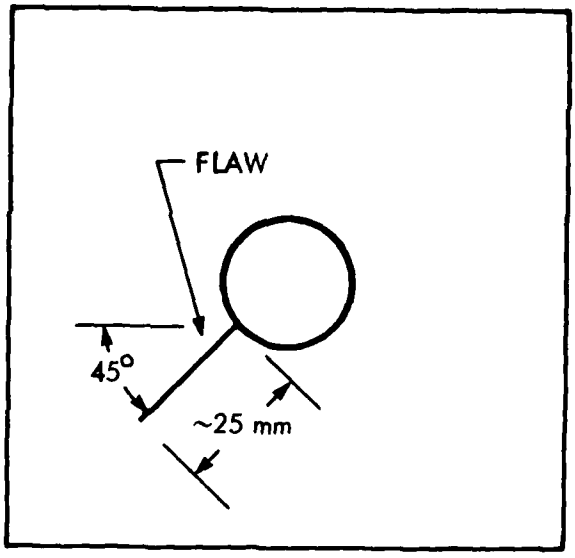

Figure 4-19. Flawed Specimen Geometry

4.9.3 Experimental Results

In these experiments, only the bottom edge of the specimen was clamped and the specimen was positioned so that it did not contact the fixture at the other two edges. The first hologram exposure was made before the plug was inserted into the hole. The plug was then cooled in liquid nitrogen and inserted and held in the hole by hand. After only a few minutes, the plug expanded sufficiently to hold itself, but about 10 minutes were required for the plug to return to room temperature at which time the second hologram exposure was made.

By using a relatively thick plate clamped only on the bottom edge, it was possible to reproduce the pattern observed by Vest, McKague and Friesem on a number of occasions. One such pattern corresponding to exposures made before and after insertion of the expanding plug for the uncracked plate is shown in Figure 4-20. Unfortunately, this pattern could not always be produced. In some cases, no fringes were apparent and, in one case, a different pattern of

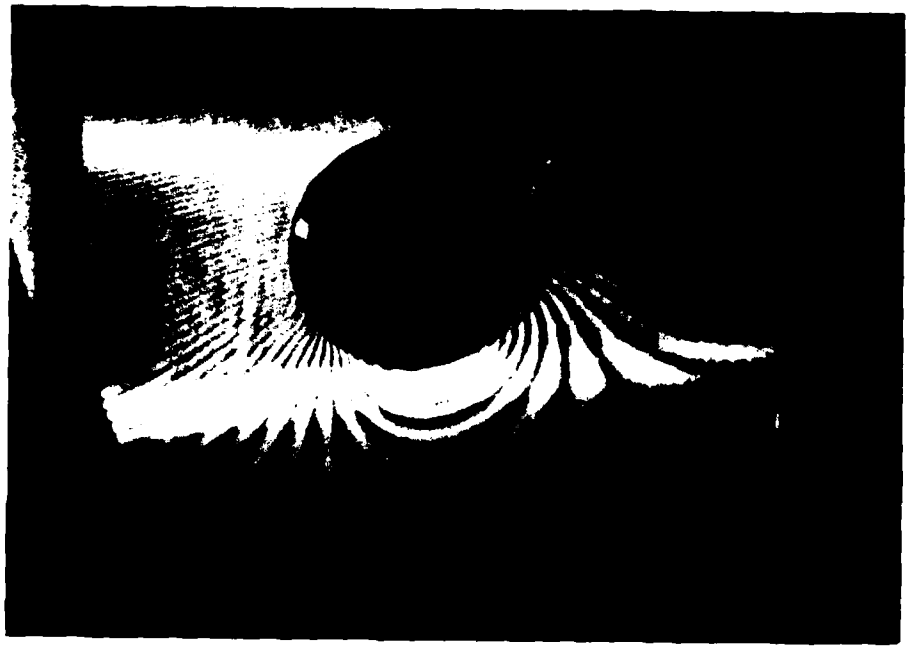

83217

Figure 4-20. Fringes Caused by the Expanding Plug in the Unflawed Specimen

fringes was obtained, as shown in Figure 4-21. It was also possible to obtain the same basic fringe pattern for the specimen with the through crack and, furthermore, to render the crack visible, as shown in Figure 4-22. Experiments have not yet been conducted to determine if the part-through crack can be made visible by use of an expanding plug.

An alternative type of loading was investigated, based on considerations described in Section 4.9.4. below. The plug was left inserted in the hole for both hologram exposures and a weight was hung from the holder used to insert the plug to produce a bending moment on the plate, as illustrated in Figure 4-23; only the bottom edge of the plate was clamped. The weight was chosen to produce about the same number of fringes in the upper part of the plate, as observed for the expanding plug case shown in Figure 4-20. The resulting interferogram for the through-cracked specimen loaded with a 300 g weight at a distance of 50 mm from the plane of the plate is shown in Figure 4-24. Although the fringe pattern does not resemble the pattern caused by the

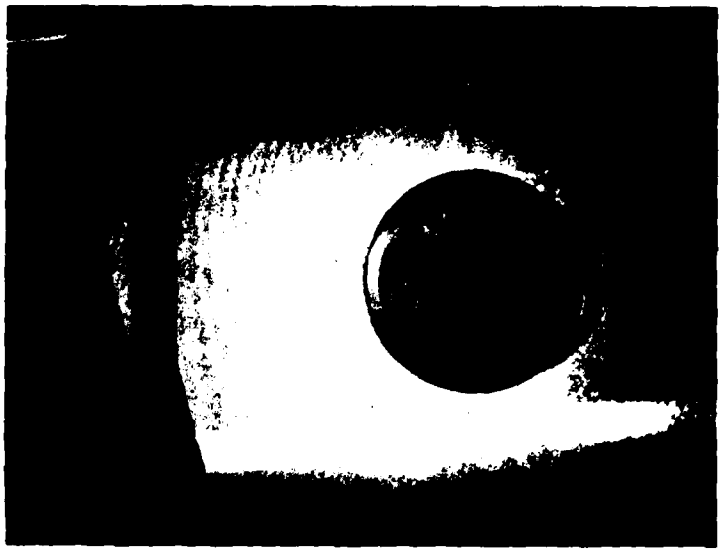

Figure 4-21. Other Fringes Caused by the Expanding Plug in the Unflawed Specimen

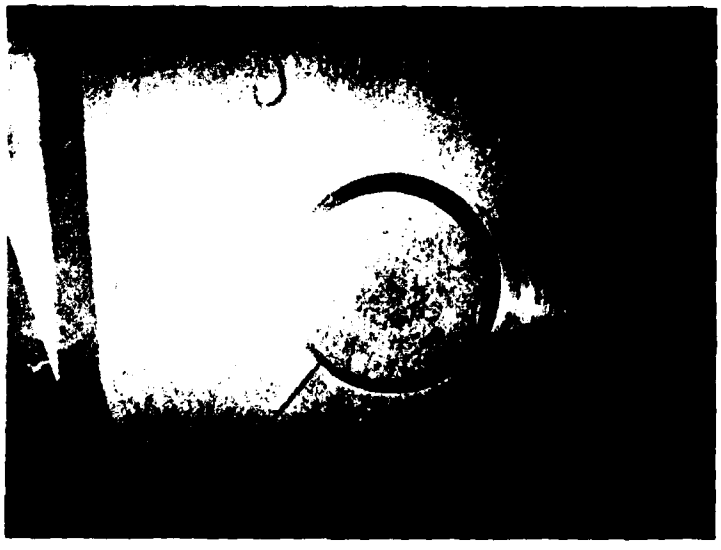

83214

Figure 4-22. Fringes Caused by the Expanding Plug in the Through-Flawed Specimen

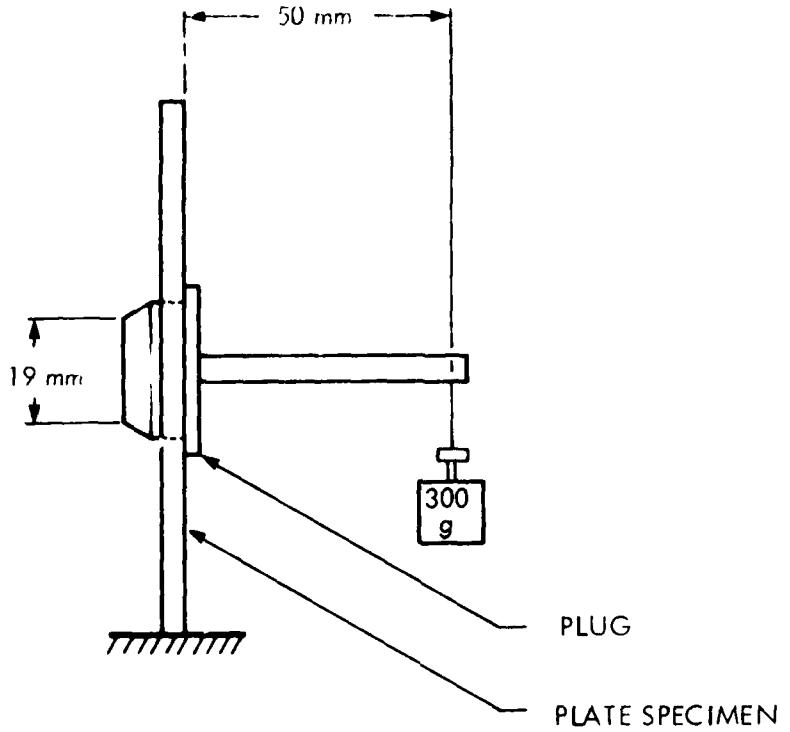

Figure 4-23. Hanging Weight Configuration

83215

Figure 4-24. Fringes Caused by the 300 g Hanging Weight

expanding plug, there is a slight fringe shift across the crack line. This indicates that an externally applied bending moment may be a useful type of loading to study fringe linearization.

4.9.4 Analysis of the Deformation Mechanism

The elastic solution for the shrink fitting of a plug into a circular hole in an infinite plate follows.

The pressure on the boundary of the hole is related to the interference fit by

$$P = \frac{\delta}{P} \left[\frac{1-V_1}{E_1} + \frac{1 + V_2}{E_2} \right]^{-1} . \qquad (4.14)$$

The distribution of radial and circumferential stress components is

$$\sigma_r = - \sigma_\theta = - P(D/2r)^2, \qquad (4.15)$$

where r is the radial distance from the hole center.

Therefore, the sum of σ_r and σ_θ is constant throughout the plate. This implies that the out-of-plane strains, and, consequently, the displacements, are also constant throughout the plate. In other words, in the absence of a crack, the analysis predicts that no fringes should be detectable with the interferometric technique. The question arises as to what the cause of the fringes in our and Vest, McKague and Friesem's experiments was, since we employed a similar type of loading. One possibility is that the stresses and deformations in a plate of finite dimensions clamped at one or all of its boundaries differs considerably from those predicted by an analysis for an infinite plate.

As it was expected that the finite dimensions of the actual plate would affect the infinite plate solution and cause the occurrence of fringes, a finite element analysis of the actual plate was carried out using the grid shown in Figure 4-25. This grid exploits the symmetry of an uncracked plate

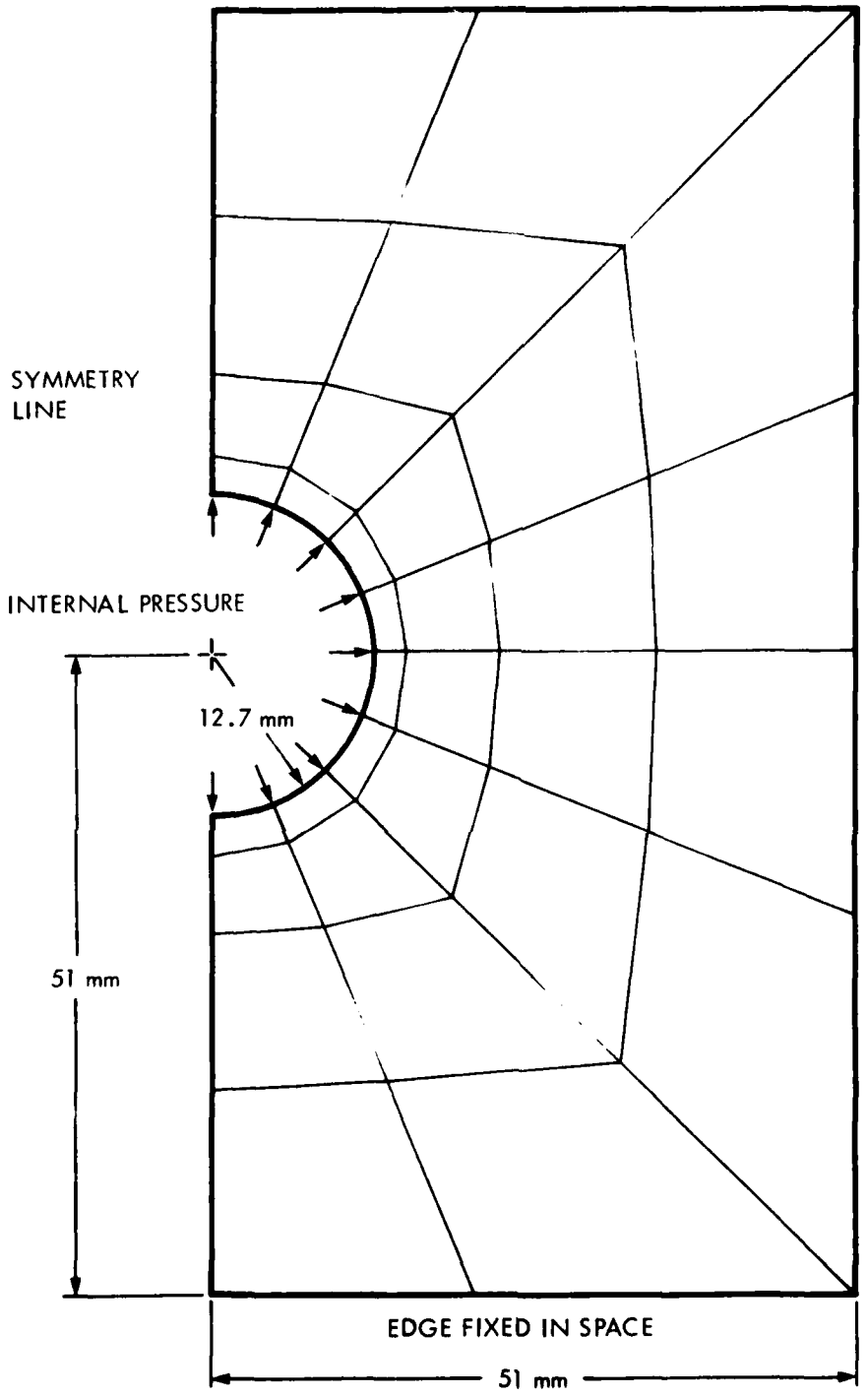

Figure 4-25. Finite Element Model of Half Specimen

8303-22

about its centerline; if the mesh is reflected through this centerline, the asymmetric problem that arises when a crack emanating from the hole is introduced may also be solved. For the uncracked plate, the lower boundary was held fixed in accord with the experimental procedure. The plate was loaded by a radial pressure of 8 psi applied outward along the inside of the hole. This pressure is representative of that encountered experimentally. The finite element results revealed that no out-of-plane displacements in excess of 0.02 microns occurs as a result of the in-plane loading of the expanding plug. Since the wavelength used here is 0.6328 microns, the calculation described predicts that no fringes at all may be detected. Therefore, because fringes are observed (Figure 4-21), a deformation mechanism involving bending of the aluminum plate was hypothesized.

If any eccentricity arises during insertion of the plug into the aluminum plate, or, if either the surface of the hole or the plug have a slight taper, the pressure at the hole boundary may not be distributed uniformly. Schematic representations of two such circumstances are shown in Figure 4-26a. Each configuration in Figure 4-26a results in the application of a bending moment to the specimen, as idealized in Figure 4-26b. Such a bending moment causes out-of-plate deflections in the specimen in a manner similar to the deflections caused by the hanging weight.

For example, using the left-hand idealization in Figure 4-26b, one may show that the deflection w(z) of the beam is given by

$$w(z) = Mz^2/2EI \qquad 0 \leq z \leq L/2 \qquad (4.16)$$

$$w(z) = ML(z-L/4)/2EI \qquad L/2 \leq z \leq L, \qquad (4.17)$$

where z is the vertical distance from the clamped edge, M is the bending moment applied at mid span, E is Young's modulus, I is the area moment of inertia and L is the length of the beam. The first equation shows that the deflection varies quadratically with z for $0 \leq z \leq L/2$, which implies that the spacing between fringes decreases as z approaches L/2, the midpoint of the beam. The

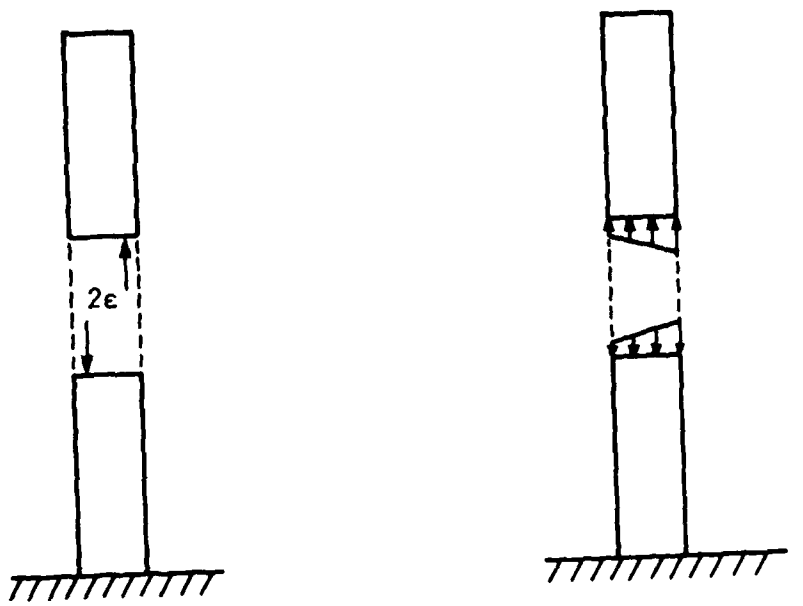

a) Nonuniform Loadings

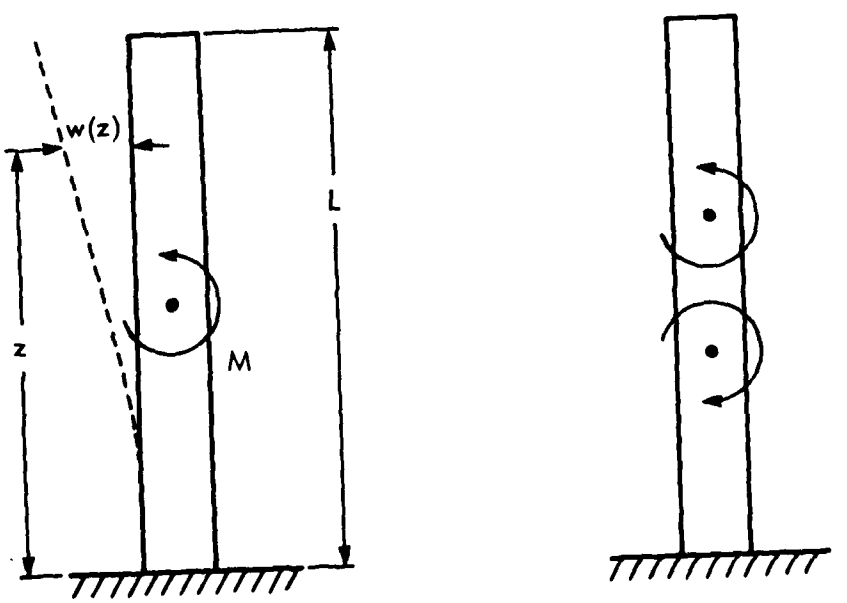

b) Idealizations

Figure 4-26. Hypothesized Out-of-Plane Loading Mechanisms

second equation shows that the deflection is linear with z for $L/2 \leq z \leq L$, which implies that the spacing between fringes is constant for this interval. Both of these phenomena are observed in Figures 4-20 and 4-24.

The bending moment required to give a certain fringe spacing or number of fringes per unit length can be calculated from the difference in out-of-plane deflection between the beam midpoint and end, z = L. The difference in deflection is

$$w(L) - w(L/2) = ML^2/4EI. \qquad (4\text{-}18)$$

Since one fringe is observed for every half-wavelength change in out-of-plane displacement, the moment required to produce N fringes per unit length in this interval is $\lambda NEI/L$ where λ is the wavelength of the light source. For $\lambda = 6.328 \times 10^{-4}$ mm, $E = 69 \times 10^3 N/mm^2$, $I = 271$ mm^4 and L = 102 mm, all corresponding to the geometry and loading configuration of Figure 4-24, the moment required is 146 Nmm. The applied moment in the experiment was actually 149 Nmm.

While this model calculation does not furnish enough detail to predict a two-dimensional fringe pattern, it clearly indicates that an out-of-plane bending mechanism can account for the number of fringes observed in the upper parts of Figure 4-20 (1.78 fringes/mm) and Figure 4-24 (1.26 fringes/mm). In fact, with an interfacial pressure of 69.0 MPa (10 psi), the left-hand non-uniform loading in Figure 4-26 can develop a moment of 150 Nmm with an eccentricity, ε, of only 17.2 μm, so that 2ε is barely one percent of the plate thickness. Future finite element calculations will permit a detailed prediction of fringe patterns based on the hypothesized loading mechanism.

4.9.5 Continuing Effort

Finite element calculations are currently being conducted to verify the suspected causes of the fringe pattern shown in Figure 4-20. If this is successful, then an attempt will be made to determine if the fringe pattern can be controlled and consistently predicted. Alternative methods of loading the

specimen in addition to the hanging weight are being investigated. One possibility is to apply a direct out-of-plane displacement to the plate with three boundaries clamped; the fourth boundary cannot be clamped with the present fixture. The displacement could be applied through a ring pressed flat against the back of the plate and concentric to the hole. Choice of a suitable displacement fixture would also permit the application of a dynamic (time varying) displacement. Other methods of dynamic loading and analysis of resulting deformations are also under consideration.

SECTION 5
RESULTS TO DATE

The results achieved thus far in the program are definitely encouraging. These results are that linear fringes can be placed across the object plane during the holographic recording step and that fringe noise is separable from the fundamental fringe frequency in the transform plane. In addition, spatial filtering produced an image laced with linear fringes without noise and also showed the presence of a known phase step in the triple exposure simulation experiment.

Other results obtained in Phase I of this program include:

- Recognizing that the filtering could not be done directly from the hologram of a reflecting object because of its surface roughness. This problem was solved by photographing the image reconstructed from the hologram in an intermediate step and linearly processing the film.

- Experimentally determining that fringe localization is easily obtained with plane waves and difficult to achieve with spherical waves.

- In addition, we determined that the FLI linear fringes, when localized with spherical waves, exhibit slight curvature over the field and a frequency shift across the field.

- Achieving reproducible holographic fringes by two methods:
  - Vest's method of the expanding plug
  - Hanging weights on the plate between exposures

  Both of these methods of stressing showed fringe shifts at the crack in the plate.

- Finite element analysis showed that fringes are not caused by deformations resulting from in-plane loading. This suggested that loading with the expanding plug causes an out-of-plane force component.

- Formulation of a model with a simple bending deformation mechanism which predicted fringe shifts agreeing with those measured in the laboratory when loaded by hanging weights on a lever arm between the exposures.

SECTION 6

6.1 FUTURE PLANS

During the coming year, we will further illustrate the FLI concept (including filtering) with a double exposure simulation experiment and transfer the experimentation to the NADC holographic system in Warminster, PA, where the static experiment will be repeated. We will then implement a beam-deflecting mechanism on the object beam of the NADC system and define a dynamic loading technique for use on this system. We will then perform experiments aimed at locating subsurface cracks in the test plates by use of the FLI concept. The deformation analysis will continue with the goal of determining sensitivity of the technique to the size, depth and location of cracks, and loading parameters in controlled experimental samples.

REFERENCES

1. Smith, H.M., Principles of Holography, Wiley-Interscience, New York (1969) pp. 194-195.

2. DeVelis, J.B. and Reynolds, G.O., Theory and Applications of Holography, Addison-Wesley, Reading, MA (1967).

3. Vest, C.M., Holographic Interferometry, John Wiley & Son, Inc., New York, NY, 1979, p. 128.

4. Reynolds, G.O., DeVelis, J.B. and Yong, Y.M., "Review of Noise Reduction Techniques in Coherent Optical Processing Systems", S.P.I.E., Vol. 52, pp. 55-81, August (1974).

5. Mueller, P.F. and Reynolds, G.O., "Image Restoration by Removal of Random Media Distortions," J. Opt. Soc. Am. 57, 1338, 1967.

6. Mueller, P.F., "Standard Microfilms for Recording Color and Multiple Images," Proceedings of the National Microfilm Association Annual Convention, May 1969.

7. Mueller, P.F., "Linear Multiple Image Storage", Appl. Opt. 8(2), 267, February 1969.

8. Goodman, J.W., Introduction to Fourier Optics, McGraw Hill, New York, NY (1968) chap. 5.

9. O'Neill, E.L., Introduction to Statistical Optics, Addison-Wesley, Reading, MA, 1963, p. 103.

10. O'Neill, E.L., IRE Trans., PGIT, 2, 1956, p. 56.

11. TRW Systems Group, "Feasibility Demonstration of Applying Advanced Holographic Systems Technology to Identify Structural Integrity of Naval Aircraft," Interim Report on Contract No. N62269-72-C-0400, 23 March 1973.

12. Vest, V.M., McKague, E.L. and Friesem, A.A., "Holographic Detection of Microcracks," J. Basic Eng. Trans ASME, (June 1971). pp. 237-241.

13. Bartolotta, C.S. and Pernick, B.J., "Holographic Nondestructive Evaluation of Interference Fit Fasteners," Applied Optics, 12, 4 (April 1973), pp. 885-886.

14. Grunewald, K. Fritzsch, W. Harnier, A.V. and Roth, E., "Nondestructive Testing of Plastics by Means of Holographic Interferometry," Polymer Eng. and Sci., 15, 1 (Jan. 1975), pp. 16-28.

15. Wang, C.T., Applied Elasticity, McGraw-Hill, New York, NY, 1953, p. 57.

APPENDIX I

MATHEMATICAL DEVELOPMENT OF BEAM SHIFTING TO CREATE THE LINEAR FRINGES OF THE HOLOGRAPHIC FLI CONCEPT

Smith[1] illustrates the principle of shifting the object wave between exposures in double-exposure holographic interferometry to create linear cosine fringes in the reconstructed interferogram. The fringes have a period, $\lambda/\delta\theta$, where $\delta\theta$ is the amount of angular shift between the object beams and λ is the wavelength of the laser light. For example, a shift of 1 degree between the beams results in a fringe pattern having a spatial frequency of 35 line pairs/mm, and a shift of 0.1 degree results in a spatial frequency of 3.5 line pairs/mm. An alternate analysis utilizing Fourier transform holography of a finite-size object is given below.

In this appendix, the Fourier transform configuration in Figure I-1 will be used, rather than the sideband Fresnel configuration of the system at NADC, in order to simplify the mathematics and illustrate the principle of linear fringes. Fourier transform holograms reconstruct by performing Fourier transforms, rather than the more complicated procedure of focussing Fresnel transforms, which is necessary for the sideband Fresnel System.

The irradiance in the hologram plane of Figure I-1 is

$$H(x) = [e^{ikx\sin(\xi o/f)} + \sim f(x,t)]^2, \qquad (I\text{-}1)$$

where $\sim$ denotes a Fourier transform.

If a prism of angle $\delta\theta$ is used to shift the direction of the object wave and another hologram is recorded on the same recording medium (note: in double-exposure hologrphic interferometry, a different state of the dynamic object, $f(x, t_1)$, is usually captured on the hologram), the irradiance of the second hologram is:

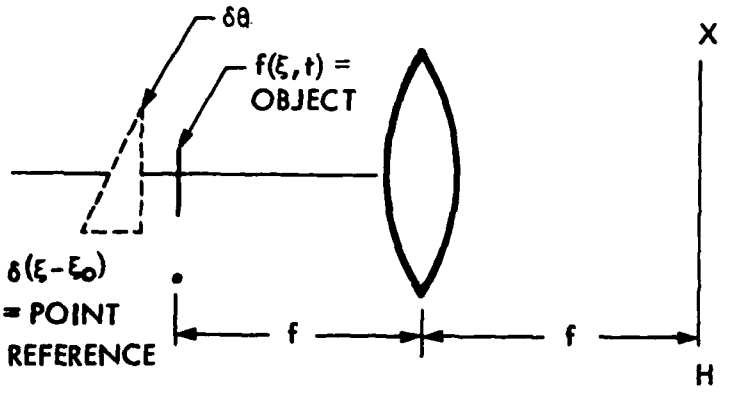

Figure I-1. Schematic of Fourier Transform Hologram System for Double-Exposure Interferometry Using a Lens of Focal Length, f.

$$H(x) = [e^{ikxsin(\xi o/f)} + -f(x-x_0,t_1]^2, \qquad (I-2)$$

where from the shift theorem of Fourier analysis $x_0 = f \tan(\delta\theta)$.

Reconstruction of the two holograms described in Equations (I-1) and (I-2) with a lens of focal length f results in a reconstructed image at the position $x' = \xi o$ of the reconstructed image plane; i.e.:

$$\text{image} = [f(x', t) + f(x', t_1)\, e^{ikx_0x'/f}]^2. \qquad (I-3)$$

If $f(x', t) = f(x', t_1)$, then

$$\text{image} = [f(x', t)]^2 \left|1+e^{ikx_0x'/f}\right|^2$$
$$= [f(x', t)]^2\ (2 + 2\cos kx_0x'/f), \qquad (I-4)$$

i.e., the image of the object is laced with "linear" cosine fringes of frequency

$$\nu = \tan \frac{\delta\theta}{\lambda}$$

Equation (I-3) shows that the linear fringes will be shifted at the positions where the stress state of the object differed between the two exposure times.

This result illustrates that the normal fringe pattern of holographic interferometry is phase-moduled onto the cosine carrier, which is created by shifting the object wave between the exposures.

APPENDIX II
MATHEMATICAL DEVELOPMENT OF LINEAR FRINGES IN A SIDEBAND FRESNEL HOLOGRAM

The purpose of this appendix is to show that linear fringes can be created in a double exposure sideband Fresnel hologram by shifting the object beam between the exposures. The mathematical development will follow that given in Chapter 3 of Reference 2.

The diffracted field emanating from an object illuminated with a tilted reference wave in the second exposure is obtained by modifying Equation 3-36 of Reference 2 to give

$$R(x) = \left[-e^{ik_1 z_1} C e^{ik_1 x^2/2z_1}\right] \int D(\xi) \exp\left(ik_1\left[\xi^2/2z_1 - \xi x/z_1\right]\right) \times e^{ik_1 \beta_0 \xi} d\xi \qquad \text{(II-1)}$$

where β_0 is the tilt angle of the beam striking the object and $\sin \beta_0 \approx \beta_0$.

The intensity distribution in the sideband Fresnel hologram produced by this wavefront is

$$I(x) = \left[k e^{ik_1 \theta x} + R(x)\right]^2 \qquad \text{(II-2)}$$

where θ is the angle between reference and object beams.

If we consider only the term in Equation II-2 corresponding to the real image, we obtain a modified version of Equation 3-81 in Reference 2. Thus,

$$I_R(x) = K'^* K C^* e^{-ik_1 z_1} e^{-ik_1 x^2/2z_1} e^{ik_1 \alpha_0 x} D^*(x), \qquad \text{(II-3)}$$

where

$$D^*(x) = \int_{z_1=0} D^*(\xi) e^{-ik_1(\xi^2/2z_1 - \xi x/z_1 + \beta_0 \xi)}\, d\xi \,. \tag{II-4}$$

When the distribution described by Equation II-3 is reconstructed with a beam of wavelength λ_2, the amplitude in the reconstructed image is given by:

$$\Psi_{imR}(\alpha) = A \int_{Z_2=0} e^{-ik_1 x^2/2z_1}\, D^*(x) e^{ik_1 x\theta} e^{ik_2 (x-\alpha)^2/2z_2}\, dx, \tag{II-5}$$

where A includes all the obliquity factors. Substituting Equation II-4 into II-5, we obtain

$$\begin{aligned}\psi_{imR}(\alpha) = {} & A e^{ik_2\alpha^2/2z_2} \int_{z_2=0} \left[\int_{z_1=0} D^*(\xi) e^{-ik_1\xi^2/2z_1} \right. \\ & \left. \times\ e^{ik_1\xi x/z_1}\ e^{-ik_1\beta_0\xi} \right] \exp\left\{ \frac{ix^2}{2} \left[\frac{k_2}{z_2} - \frac{k_1}{z_1} \right] \right\} \\ & \times\ e^{ik_1 x\theta} e^{ik_2 x\alpha/z_2}\, dx,\end{aligned} \tag{II-6}$$

which is a modified version of Equation 3-84 in Reference 2.

Applying the focussing condition $k_1 z_2 = k_2 z_1$ to Equation II-6 yields

$$\begin{aligned}\psi_{imR}(\alpha) = {} & A e^{ik_2\alpha^2/2z_2} \int_{z_2=0} \left[\int_{z_1=0} D^*(\xi) e^{-ik_1\xi_1^2/2z_1} \right. \\ & \left. \times\ e^{ik_1\xi(x/z_1 - \beta_0)}\, d\xi \right] e^{ix(k_1\theta - k_2\alpha/z_2)}\, dx \,.\end{aligned} \tag{II-7}$$

In Equation II-7, the ξ integral is the Fourier transform of a Fresnel wavefront. This gives

$$\psi_{imR}(\alpha) = Ae^{ik_2\alpha^2/2z_2} \int_{z_1=0} D^*\left(-\frac{x}{\lambda_1 z_1} + \frac{\beta_o}{\lambda}\right) e^{ik_1/2z_1\left(\beta_o - \frac{x}{z_1}\right)^2}$$

$$\times\ e^{2\pi i x\left(\frac{\theta}{\lambda_1} - \frac{\alpha}{\lambda_2 z_2}\right)}\, dx, \qquad \text{(II-8)}$$

where tilda denotes a Fourier transform operation.

Making the change of variable

$$x' = \frac{x}{\lambda_1 z_1} + \beta_o/\lambda \qquad \text{(II-9)}$$

and carrying out the Fourier transform operation indicated in Equation II-8, we get,

$$\psi_{imR}(\alpha) = Ae^{ik_2\alpha^2/2z_2}\ e^{2\pi i\left(\frac{\beta_o\theta z_1}{\lambda_1} - \frac{\alpha\beta_o z_1}{\lambda_2 z_2}\right)}$$

$$\times\ (-\lambda_1 z_1)\ D^*\ (\alpha - z_1\theta)e^{-2\pi i/2z_1)(\alpha - z_1\theta)^2}\ . \qquad \text{(II-10)}$$

A comparison of Equation II-10 with Equation 3-89 in Reference 2 shows that the only difference between the reconstructed image of a sideband Fresnel hologram and one created with a tilted object wave is the linear phase factor (LPF) in α, i.e.,

$$LPF = e^{2\pi i\left(\beta_o \frac{\theta}{\lambda} z_1 - \frac{\alpha\beta_o z_1}{\lambda_2 z_2}\right)}. \qquad \text{(II-11)}$$

Equation II-11 shows that the phase factor resulting from the tip is linear in α and has a frequency proportional to the tip angle β_o, the hologram construction distance, z_1, the reconstruction distance, z_2, and the reconstruction wavelength, λ_2.

Thus, if a double exposure hologram were made in which the only difference was a tilt of the object beam in one of the exposures, then the reconstructed image would be laced with linear cosine fringes of the form,

$$1 + \cos 2\pi \left(\frac{\beta_0 z_1}{\lambda_1} - \frac{\alpha\beta_0 z_1}{\lambda_2 z_2} \right) . \qquad \text{(II-12)}$$

This shows that tilting the object beam in the hologram results in linear fringes across the image. The analysis of the virtual image yields a similar result.

APPENDIX III
COMPUTER STUDY OF FRINGES PRODUCED BY TWO COHERENT SPHERICAL WAVES

A. DISCUSSION

This study calculates the fringes produced on a one square meter screen at a distance two meters from two coherent point sources. These dimensions correspond to the physical arrangement of the NADC holographic system. The specimen under evaluation is approximately one square meter at a distance of two meters. The specimen is illuminated with a spherically expanding laser beam pulse in the double exposure, holographic interferometer system.

The reconstruction of the double exposure hologram with the source shifted between exposures produces an image of the specimen with identical fringes to those fringes produced when the specimen is illuminated by two coherent sources, as in Figure III-1.

In our experiments, we changed the optical path of the laser illumination by inserting a mirror in the beam. The mirror was tipped between the two exposures with the result that the apparent source position changed between the exposures.

The calculation of the fringe pattern requires only a calculation of the optical path from each source to points on the screen. When the path difference, δp, is an even multiple of the half wavelengths, a bright point results. When δp is an odd multiple of the wavelength, a minimum results. A calculation of the change of path difference in an interval divided by the wavelength is a measure of the number of fringes in the interval. The computer study determines δp in 5 mm intervals each, 10 centimeters along a horizontal line at the center of the test specimen and at the top of the test specimen.

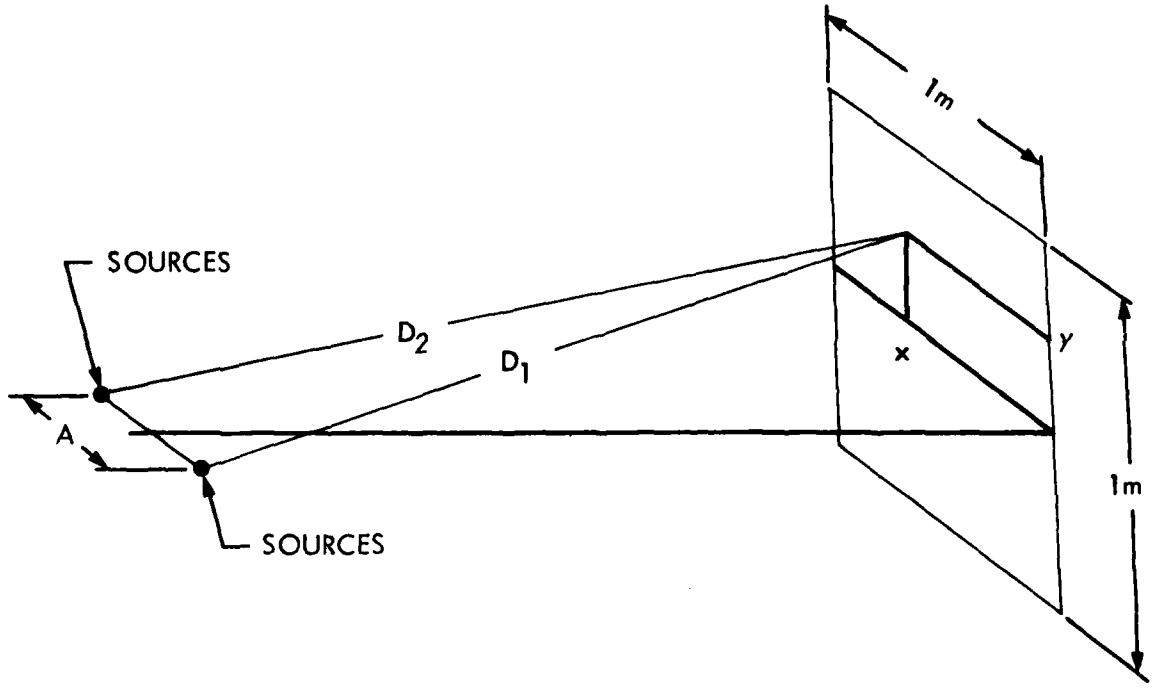

Figure III-1. Coordinate System for Source and Screen

The results show that for a source, off-axis 0.4 meters, the fringe frequency will change by 24% from the center of one edge of the specimen to the far corners. This may be a larger frequency shift than we can tolerate in our filtering system, which will force us to implement the plane wave solution. The computer program used to obtain this result is given below.

B. PROGRAM FOR OPTICAL PATH DIFFERENCE COMPUTATION

```
*LIST

5 S= .005
10 PRINT "THE RANGE IS 2 METERS"
21 A=2*S*100
25 PRINT
26 PRINT
30 PRINT "THE SOURCE SEPARATION IS"A"CENTIMETERS"
35 PRINT "X", "Y", "D1", "D2", "D1-D2"
36 PRINT " ", " ", "METERS","METERS","MILLIMETERS"
40 X=0
50 Y=0
99 PRINT
100 GOSUB 400
110 M=(D-E)*1000
120 PRINT X,Y,D,E,M
130 X=X+.005
140 GOSUB 400
150 N=(D-E)*1000
155 L=(N-M)*1000
160 PRINT X,Y,D,E,N
170 PRINT "DIFFERENCE CHANGE IN 5MM INTERVAL IS"L"MICRONS"
175 PRINT "THIS EQUALS A CHANGE OF"L/.6328"FRINGES AT .6328 MICRONS"
176PRINT "IN THE 5MM INTERVAL."
180 X=X+.095
190 IF X>.95 THEN 800
195 GOTO 100
400 D=-2+(SQR(4+(X+S)**2+Y**2))
410 E=-2+SQR(4+(X-S)**2+Y**2)
420 RETURN
800 Y=Y+.5
810 X=0
820 IF Y=1 THEN 850
830 GOTO 99
850 S=S*2
860 IF S=.16 THEN 900
870 GOTO 21
900 END
```

PROGRAM FOR OPTICAL PATH DIFFERENCE COMPUTATION (Continued)

```
#RUN


THE RANGE IS 2 METERS

THE SOURCE SEPARATION IS     1 CENTIMETERS
X                Y                D1                D2                D1-D2
                                  METERS            METERS            MILLIMETERS

            0                0          6.24358e-06       6.24358e-06
            0
         .005                0          2.49891e-05                 0
    .0249891
DIFFERENCE CHANGE IN 5MM INTERVAL IS    24.98909 MICRONS
THIS EQUALS A CHANGE OF    39.48971 FRINGES AT .6328 MICRONS
IN THE 5MM INTERVAL
           .1                0          .0027543          .002255          .4993682
         .105                0          .0030227          .0024984          .524274
DIFFERENCE CHANGE IN 5MM INTERVAL IS    24.90586 MICRONS
THIS EQUALS A CHANGE OF    39.35819 FRINGES AT .6328 MICRONS
IN THE 5MM INTERVAL
           .2                0          .0104788          .0094838          .9950362
         .205                0          .0109948          .0099751          1.019661
DIFFERENCE CHANGE IN 5MM INTERVAL IS    24.62439 MICRONS
THIS EQUALS A CHANGE OF    38.91339 FRINGES AT .6328 MICRONS
IN THE 5MM INTERVAL
           .3                0          .0231226          .0216392          1.483396
         .305                0          .0238824          .0223748          1.507566
DIFFERENCE CHANGE IN 5MM INTERVAL IS    24.16968 MICRONS
THIS EQUALS A CHANGE OF    38.19482 FRINGES AT .6328 MICRONS
IN THE 5MM INTERVAL
           .4                0          .0405943          .0386331          1.961145
         .405                0          .0415925          .0396078          1.984704
DIFFERENCE CHANGE IN 5MM INTERVAL IS    23.55874 MICRONS
THIS EQUALS A CHANGE OF    37.22935 FRINGES AT .6328 MICRONS
IN THE 5MM INTERVAL
           .5                0          .0627712          .0603458          2.425347
         .505                0          .064001           .0615528          2.448158
DIFFERENCE CHANGE IN 5MM INTERVAL IS    22.81088 MICRONS
THIS EQUALS A CHANGE OF    36.04753 FRINGES AT .6328 MICRONS
IN THE 5MM INTERVAL
           .6                0          .0895035            .08663          2.826477
         .605                0          .0909567          .0880613          2.895412
DIFFERENCE CHANGE IN 5MM INTERVAL IS    21.93543 MICRONS
THIS EQUALS A CHANGE OF    34.66408 FRINGES AT .6328 MICRONS
IN THE 5MM INTERVAL
           .7                0           .120619          .1173155          3.303495
         .705                0          .1222865           .118962          3.324483
DIFFERENCE CHANGE IN 5MM INTERVAL IS    20.98736 MICRONS
THIS EQUALS A CHANGE OF    33.16587 FRINGES AT .6328 MICRONS
IN THE 5MM INTERVAL
           .8                0          .1559279           .152214          3.713891
         .805                0          .1577998          .1540659          3.733879
DIFFERENCE CHANGE IN 5MM INTERVAL IS    19.98803 MICRONS
THIS EQUALS A CHANGE OF    31.58665 FRINGES AT .6328 MICRONS
IN THE 5MM INTERVAL
           .9                0          .1952278          .1911241          4.103638
         .905                0          .1972938          .1931712          4.122576
DIFFERENCE CHANGE IN 5MM INTERVAL IS    18.93747 MICRONS
THIS EQUALS A CHANGE OF    29.92647 FRINGES AT .6328 MICRONS
IN THE 5MM INTERVAL
```

PROGRAM FOR OPTICAL PATH DIFFERENCE COMPUTATION (Continued)

```
          0                .5          .0615589          .0615589                  0
       .005                .5          .0615771          .0615528          .0242433
DIFFERENCE CHANGE IN 5MM INTERVAL IS    24.24376 MICRONS
THIS EQUALS A CHANGE OF   38.31109 FRINGES AT .6328 MICRONS
IN THE 5MM INTERVAL
         .1                .5           .064225          .0637405          .4844936
       .105                .5          .0644854          .0639767          .5086614
DIFFERENCE CHANGE IN 5MM INTERVAL IS    24.16782 MICRONS
THIS EQUALS A CHANGE OF   38.19188 FRINGES AT .6328 MICRONS
IN THE 5MM INTERVAL
         .2                .5          .0717203          .0707547          .9656083
       .205                .5           .072221          .0712315          .9895191
DIFFERENCE CHANGE IN 5MM INTERVAL IS    23.91078 MICRONS
THIS EQUALS A CHANGE OF   37.78568 FRINGES AT .6328 MICRONS
IN THE 5MM INTERVAL
         .3                .5          .0839926          .0825525          1.440038
       .305                .5          .0847302          .0832667          1.463532
DIFFERENCE CHANGE IN 5MM INTERVAL IS    23.49448 MICRONS
THIS EQUALS A CHANGE OF   37.12782 FRINGES AT .6328 MICRONS
IN THE 5MM INTERVAL
         .4                .5          .1009581          .0990534          1.904747
       .405                .5          .1019277                .1           1.92768
DIFFERENCE CHANGE IN 5MM INTERVAL IS    22.93381 MICRONS
THIS EQUALS A CHANGE OF 36.2418 FRINGES AT .6328 MICRONS
IN THE 5MM INTERVAL
         .5                .5          .1225044          .1201474          2.357014
       .505                .5          .1236996          .1213203          2.379261
DIFFERENCE CHANGE IN 5MM INTERVAL IS    22.24651 MICRONS
THIS EQUALS A CHANGE OF   35.15567 FRINGES AT .6328 MICRONS
IN THE 5MM INTERVAL
         .6                .5          .1484937          .1456992          2.794478
       .605                .5           .149907           .147091          2.815915
DIFFERENCE CHANGE IN 5MM INTERVAL IS    21.43217 MICRONS
THIS EQUALS A CHANGE OF   33.87669 FRINGES AT .6328 MICRONS
IN THE 5MM INTERVAL
         .7                .5          .1787668          .1755516          3.215197
       .705                .5          .1803899          .1771541          3.235757
DIFFERENCE CHANGE IN 5MM INTERVAL IS    20.55988 MICRONS
THIS EQUALS A CHANGE OF   32.49032 FRINGES AT .6328 MICRONS
IN THE 5MM INTERVAL
         .8                .5          .2131482          .2095305          3.617709
       .805                .5          .2149718          .2113344          3.637344
DIFFERENCE CHANGE IN 5MM INTERVAL IS    19.63416 MICRONS
THIS EQUALS A CHANGE OF   31.02743 FRINGES AT .6328 MICRONS
IN THE 5MM INTERVAL
         .9                .5          .2514495          .2474485           4.00098
       .905                .5           .253464          .2494443          4.019627
DIFFERENCE CHANGE IN 5MM INTERVAL IS    18.64696 MICRONS
THIS EQUALS A CHANGE OF   29.46738 FRINGES AT .6328 MICRONS
IN THE 5MM INTERVAL
```

PROGRAM FOR OPTICAL PATH DIFFERENCE COMPUTATION (Continued)

```
THE SOURCE SEPARATION IS      2 CENTIMETERS
X                  Y          D1                D2                D1-D2
                              METERS            METERS            MILLIMETERS

          0                   0          2.49891e-05       2.49891e-05
          0
       .005                   0          5.62362e-05       6.24358e-06
    .0499926
DIFFERENCE CHANGE IN 5MM INTERVAL IS    49.99261 MICRONS
THIS EQUALS A CHANGE OF    79.00223 FRINGES AT .6328 MICRONS
IN THE 5MM INTERVAL
         .1                   0          .0030227          .002024          .9987419
        .105                  0          .0033035          .002255          1.048538
DIFFERENCE CHANGE IN 5MM INTERVAL IS    49.79638 MICRONS
THIS EQUALS A CHANGE OF    78.69213 FRINGES AT .6328 MICRONS
IN THE 5MM INTERVAL
         .2                   0          .010994           .0090047         1.990054
        .205                  0          .011523           .0094838         2.039288
DIFFERENCE CHANGE IN 5MM INTERVAL IS    49.23678 MICRONS
THIS EQUALS A CHANGE OF    77.80306 FRINGES AT .6328 MICRONS
IN THE 5MM INTERVAL
         .3                   0          .0238824          .0209156          2.96678
        .305                  0          .0246543          .0216392         3.015105
DIFFERENCE CHANGE IN 5MM INTERVAL IS    48.32518 MICRONS
THIS EQUALS A CHANGE OF    76.36723 FRINGES AT .6328 MICRONS
IN THE 5MM INTERVAL
         .4                   0          .0415925          .0376702         3.922271
        .405                  0          .0426025          .0386331         3.969373
DIFFERENCE CHANGE IN 5MM INTERVAL IS    47.10257 MICRONS
THIS EQUALS A CHANGE OF    74.43516 FRINGES AT .6328 MICRONS
IN THE 5MM INTERVAL
         .5                   0           .064001          .0591503         4.850654
        .505                  0          .0652421          .0603458          4.89626
DIFFERENCE CHANGE IN 5MM INTERVAL IS    45.60643 MICRONS
THIS EQUALS A CHANGE OF    72.07085 FRINGES AT .6328 MICRONS
IN THE 5MM INTERVAL
         .6                   0          .0909567          .0852098         5.746894
        .605                  0          .0924208           .08663          5.790793
DIFFERENCE CHANGE IN 5MM INTERVAL IS    43.89882 MICRONS
THIS EQUALS A CHANGE OF    69.37235 FRINGES AT .6328 MICRONS
IN THE 5MM INTERVAL
         .7                   0          .1222865          .1156795         6.606956
        .705                  0          .1239644          .1173155         6.648929
DIFFERENCE CHANGE IN 5MM INTERVAL IS    41.97282 MICRONS
THIS EQUALS A CHANGE OF    66.32872 FRINGES AT .6328 MICRONS
IN THE 5MM INTERVAL
         .8                   0          .1577998           .150372         7.427245
        .805                  0          .1596817          .1522139         7.467722
DIFFERENCE CHANGE IN 5MM INTERVAL IS    39.97791 MICRONS
THIS EQUALS A CHANGE OF    63.17621 FRINGES AT .6328 MICRONS
IN THE 5MM INTERVAL
         .9                   0          .1972948          .1890865         8.207226
        .905                  0          .1993692          .1911241         8.245084
DIFFERENCE CHANGE IN 5MM INTERVAL IS    37.85825 MICRONS
THIS EQUALS A CHANGE OF    59.82656 FRINGES AT .6328 MICRONS
IN THE 5MM INTERVAL
```

PROGRAM FOR OPTICAL PATH DIFFERENCE COMPUTATION (Continued)

```
          0                .5          .0615771          .0615771                0
       .005                .5          .0616074          .0615589            .0485
DIFFERENCE CHANGE IN 5MM INTERVAL IS    48.50002 MICRONS
THIS EQUALS A CHANGE OF   76.64352 FRINGES AT .6328 MICRONS
IN THF 5MM INTERVAL
          .1                .5          .0644854          .0635164         .9689936
       .105                .5          .0647578          .0637405         1.017314
DIFFERENCE CHANGE IN 5MM INTERVAL IS    48.32073 MICRONS
THIS EQUALS A CHANGE OF 76.3602 FRINGES AT .6328 MICRONS
IN THE 5MM INTERVAL
          .2                .5           .072221          .0702898           1.9312
       .205                .5          .0727337          .0707547         1.979006
DIFFERENCE CHANGE IN 5MM INTERVAL IS    47.80665 MICRONS
THIS EQUALS A CHANGE OF 75.5478 FRINGES AT .6328 MICRONS
IN THE 5MM INTERVAL
          .3                .5          .0847302          .0818501         2.880066
       .305                .5          .0854796          .0825525          2.92704
DIFFERENCE CHANGE IN 5MM INTERVAL IS    46.97406 MICRONS
THIS EQUALS A CHANGE OF   74.23208 FRINGES AT .6328 MICRONS
IN THE 5MM INTERVAL
          .4                .5          .1019277          .0981182         3.809475
       .405                .5          .1029087          .0990534         3.855329
DIFFERENCE CHANGE IN 5MM INTERVAL IS    45.85367 MICRONS
THIS EQUALS A CHANGE OF   72.46156 FRINGES AT .6328 MICRONS
IN THF 5MM INTERVAL
          .5                .5          .1236996          .1189856         4.713992
       .505                .5          .1249059          .1201474         4.758469
DIFFERENCE CHANGE IN 5MM INTERVAL IS    44.47716 MICRONS
THIS EQUALS A CHANGE OF   70.28629 FRINGES AT .6328 MICRONS
IN THE 5MM INTERVAL
          .6                .5           .149907          .1443181         5.588898
       .605                .5          .151331           .1456992         5.631803
DIFFERENCE CHANGE IN 5MM INTERVAL IS    42.90414 MICRONS
THIS EQUALS A CHANGE OF   67.80047 FRINGES AT .6328 MICRONS
IN THE 5MM INTERVAL
          .7                .5          .1803899          .1739595         6.430365
       .705                .5          .1820231          .1755516         6.471483
DIFFERENCE CHANGE IN 5MM INTERVAL IS    41.11785 MICRONS
THIS EQUALS A CHANGE OF   64.97763 FRINGES AT .6328 MICRONS
IN THE 5MM INTERVAL
          .8                .5          .2149718          .2077364         7.235387
       .805                .5          .2168051          .2095305          7.27465
DIFFERENCE CHANGE IN 5MM INTERVAL IS    39.26271 MICRONS
THIS EQUALS A CHANGE OF   62.04401 FRINGES AT .6328 MICRONS
IN THF 5MM INTERVAL
          .9                .5           .253464          .2454621          8.00191
       .905                .5          .2554877          .2474485         8.039195
DIFFERENCE CHANGE IN 5MM INTERVAL IS    37.28461 MICRONS
THIS EQUALS A CHANGE OF   58.92006 FRINGES AT .6328 MICRONS
IN THF 5MM INTERVAL
```

PROGRAM FOR OPTICAL PATH DIFFERENCE COMPUTATION (Continued)

```
THE SOURCE SEPARATION IS     4 CENTIMETERS
X                 Y                 D1                D2                D1-D2
                                    METERS            METERS            MILLIMETERS

          0                         0                 .0001             .0001                    0
       .005                         0               .0001562          5.62362e-05
   .0999964
DIFFERENCE CHANGE IN 5MM INTERVAL IS    99.99638 MICRONS
THIS EQUALS A CHANGE OF    158.0221 FRINGES AT .6328 MICRONS
IN THE 5MM INTERVAL
          .1                        0               .0035968          .0015994              1.997394
        .105                        0               .0039024          .0018054              2.096998
DIFFERENCE CHANGE IN 5MM INTERVAL IS   99.604 MICRONS
THIS EQUALS A CHANGE OF 157.402 FRINGES AT .6328 MICRONS
IN THE 5MM INTERVAL
          .2                        0               .0120636          .0080837              3.979962
        .205                        0               .0126164          .008538               4.078426
DIFFERENCE CHANGE IN 5MM INTERVAL IS    98.46368 MICRONS
THIS EQUALS A CHANGE OF    155.6 FRINGES AT .6328 MICRONS
IN THE 5MM INTERVAL
          .3                        0               .0254382          .0195049              5.933332
        .305                        0               .0262342          .0202042              6.029993
DIFFERENCE CHANGE IN 5MM INTERVAL IS    96.66175 MICRONS
THIS EQUALS A CHANGE OF    152.7524 FRINGES AT .6328 MICRONS
IN THE 5MM INTERVAL
          .4                        0               .0436242          .0357799              7.844284
        .405                        0               .0446577          .0367192                7.9385
DIFFERENCE CHANGE IN 5MM INTERVAL IS    94.21629 MICRONS
THIS EQUALS A CHANGE OF    148.8879 FRINGES AT .6328 MICRONS
IN THE 5MM INTERVAL
          .5                        0               .0664946          .0567936                9.701
        .505                        0               .0677584          .0579662              9.792211
DIFFERENCE CHANGE IN 5MM INTERVAL IS    91.21096 MICRONS
THIS EQUALS A CHANGE OF    144.1387 FRINGES AT .6328 MICRONS
IN THE 5MM INTERVAL
          .6                        0               .0938959          .0824025              11.49343
        .605                        0               .0953818          .0838006              11.58121
DIFFERENCE CHANGE IN 5MM INTERVAL IS    87.78369 MICRONS
THIS EQUALS A CHANGE OF    138.7227 FRINGES AT .6328 MICRONS
IN THE 5MM INTERVAL
          .7                        0               .1256528          .1124393              13.21349
        .705                        0               .1273516          .1140541              13.29748
DIFFERENCE CHANGE IN 5MM INTERVAL IS    83.98676 MICRONS
THIS EQUALS A CHANGE OF    132.7224 FRINGES AT .6328 MICRONS
IN THE 5MM INTERVAL
          .8                        0               .1615735          .1467184              14.85508
        .805                        0               .1634752          .1485402                14.935
DIFFERENCE CHANGE IN 5MM INTERVAL IS    79.92435 MICRONS
THIS EQUALS A CHANGE OF    126.3027 FRINGES AT .6328 MICRONS
IN THE 5MM INTERVAL
          .9                        0                .201454           .18504               16.41401
        .905                        0               .2035483          .1870585              16.48976
DIFFERENCE CHANGE IN 5MM INTERVAL IS    75.74439 MICRONS
THIS EQUALS A CHANGE OF    119.6972 FRINGES AT .6328 MICRONS
IN THE 5MM INTERVAL
```

PROGRAM FOR OPTICAL PATH DIFFERENCE COMPUTATION (Continued)

```
          0                .5          .0616498          .0616498                  0
       .005                .5          .0617044          .0616074         .0970112
DIFFERENCE CHANGE IN 5MM INTERVAL IS    97.01122 MICRONS
THIS EQUALS A CHANGE OF   153.3047 FRINGES AT .6328 MICRONS
IN THE 5MM INTERVAL
          .1                .5          .0650424          .0631045         1.937905
       .105                .5          .0653389          .0633044         2.034558
DIFFERENCE CHANGE IN 5MM INTERVAL IS    96.65264 MICRONS
THIS EQUALS A CHANGE OF   152.7381 FRINGES AT .6328 MICRONS
IN THE 5MM INTERVAL
          .2                .5          .0732583           .069396         3.862266
       .205                .5          .0737948          .0698369         3.957876
DIFFERENCE CHANGE IN 5MM INTERVAL IS    95.60958 MICRONS
THIS EQUALS A CHANGE OF   151.0897 FRINGES AT .6328 MICRONS
IN THE 5MM INTERVAL
          .3                .5          .0862406          .0804807         5.759921
       .305                .5          .0870134          .0811595         5.853883
DIFFERENCE CHANGE IN 5MM INTERVAL IS    93.96207 MICRONS
THIS EQUALS A CHANGE OF   148.4862 FRINGES AT .6328 MICRONS
IN THE 5MM INTERVAL
          .4                .5          .1039011          .0962824         7.618716
       .405                .5           .104905          .0971945         7.710434
DIFFERENCE CHANGE IN 5MM INTERVAL IS    91.71855 MICRONS
THIS EQUALS A CHANGE OF   144.9408 FRINGES AT .6328 MICRONS
IN THE 5MM INTERVAL
          .5                .5          .1261232          .1166955         9.427699
       .505                .5          .1273516           .117835         9.516653
DIFFERENCE CHANGE IN 5MM INTERVAL IS    88.95338 MICRONS
THIS EQUALS A CHANGE OF   140.5711 FRINGES AT .6328 MICRONS
IN THE 5MM INTERVAL
          .6                .5          .1527657          .1415882         11.17746
       .605                .5           .154211          .1429477         11.26325
DIFFERENCE CHANGE IN 5MM INTERVAL IS    85.79159 MICRONS
THIS EQUALS A CHANGE OF   135.5746 FRINGES AT .6328 MICRONS
IN THE 5MM INTERVAL
          .7                .5          .1836666          .1708063         12.86034
       .705                .5          .1853203          .1723777         12.94261
DIFFERENCE CHANGE IN 5MM INTERVAL IS    82.27491 MICRONS
THIS EQUALS A CHANGE OF   130.0172 FRINGES AT .6328 MICRONS
IN THE 5MM INTERVAL
          .8                .5          .2186482          .2041778         14.47039
       .805                .5           .220501          .2059522         14.54888
DIFFERENCE CHANGE IN 5MM INTERVAL IS    78.49741 MICRONS
THIS EQUALS A CHANGE OF   124.0477 FRINGES AT .6328 MICRONS
IN THE 5MM INTERVAL
          .9                .5          .2575207          .2415173         16.00341
       .905                .5           .259563           .243485         16.07801
DIFFERENCE CHANGE IN 5MM INTERVAL IS    74.59521 MICRONS
THIS EQUALS A CHANGE OF   117.8812 FRINGES AT .6328 MICRONS
IN THE 5MM INTERVAL
```

PROGRAM FOR OPTICAL PATH DIFFERENCE COMPUTATION (Continued)

```
THE SOURCE SEPARATION IS     8 CENTIMETERS
X              Y             D1                D2                D1-D2
                             METERS            METERS            MILLIMETERS

          0                  0          .0004          .0004          0
       .005                  0        .0005062       .0003062       .1999479
DIFFERENCE CHANGE IN 5MM INTERVAL IS    199.9479 MICRONS
THIS EQUALS A CHANGE OF    315.9732 FRINGES AT .6328 MICRONS
IN THE 5MM INTERVAL
         .1                  0         .004894        .000898       3.994223
       .105                  0        .0052493        .001056       4.193386
DIFFERENCE CHANGE IN 5MM INTERVAL IS    199.1638 MICRONS
THIS EQUALS A CHANGE OF    314.7341 FRINGES AT .6328 MICRONS
IN THE 5MM INTERVAL
         .2                  0        .0143485       .0063898       7.958739
       .205                  0        .0149504       .0067947       8.155668
DIFFERENCE CHANGE IN 5MM INTERVAL IS    196.9298 MICRONS
THIS EQUALS A CHANGE OF    311.2038 FRINGES AT .6328 MICRONS
IN THE 5MM INTERVAL
         .3                  0        .0286942       .0168292       11.86498
       .305                  0        .0295381       .0174798       12.05827
DIFFERENCE CHANGE IN 5MM INTERVAL IS    193.2979 MICRONS
THIS EQUALS A CHANGE OF    305.4644 FRINGES AT .6328 MICRONS
IN THE 5MM INTERVAL
         .4                  0        .0478281       .0321417       15.60638
       .405                  0        .0489082       .0330334        15.8748
DIFFERENCE CHANGE IN 5MM INTERVAL IS    188.4252 MICRONS
THIS EQUALS A CHANGE OF    297.7642 FRINGES AT .6328 MICRONS
IN THE 5MM INTERVAL
         .5                  0        .0716177       .0522183       19.39942
       .505                  0        .0729267       .0533448       19.58184
DIFFERENCE CHANGE IN 5MM INTERVAL IS    182.4181 MICRONS
THIS EQUALS A CHANGE OF    288.2713 FRINGES AT .6328 MICRONS
IN THE 5MM INTERVAL
         .6                  0        .0999047       .0769208       22.98397
       .605                  0         .101434       .0782745        23.1595
DIFFERENCE CHANGE IN 5MM INTERVAL IS    175.5376 MICRONS
THIS EQUALS A CHANGE OF    277.3982 FRINGES AT .6328 MICRONS
IN THE 5MM INTERVAL
         .7                  0        .1325102       .1060864       26.42384
       .705                  0        .1342504       .1076586        26.5918
DIFFERENCE CHANGE IN 5MM INTERVAL IS 167.964 MICRONS
THIS EQUALS A CHANGE OF    265.4298 FRINGES AT .6328 MICRONS
IN THE 5MM INTERVAL
         .8                  0        .1692395       .1395326       29.70683
       .805                  0        .1711805       .1413138        29.8667
DIFFERENCE CHANGE IN 5MM INTERVAL IS    159.8709 MICRONS
THIS EQUALS A CHANGE OF    252.6404 FRINGES AT .6328 MICRONS
IN THE 5MM INTERVAL
         .9                  0        .2098869       .1770622       32.82465
       .905                  0        .2120183       .1790422       32.97609
DIFFERENCE CHANGE IN 5MM INTERVAL IS    151.4444 MICRONS
THIS EQUALS A CHANGE OF    239.3243 FRINGES AT .6328 MICRONS
IN THE 5MM INTERVAL
```

PROGRAM FOR OPTICAL PATH DIFFERENCE COMPUTATION (Continued)

```
          0                .5          .0619408          .0619408                0
        .005               .5          .0620439          .0618499         .1939805
DIFFERENCE CHANGE IN 5MM INTERVAL IS   193.9805 MICRONS
THIS EQUALS A CHANGE OF   306.5432 FRINGES AT .6328 MICRONS
IN THE 5MM INTERVAL
         .1                .5           .066301          .0624257         3.875295
        .105               .5          .0666458          .0625773         4.068559
DIFFERENCE CHANGE IN 5MM INTERVAL IS   193.2643 MICRONS
THIS EQUALS A CHANGE OF   305.4114 FRINGES AT .6328 MICRONS
IN THE 5MM INTERVAL
         .2                .5          .0754758          .0677524         7.723447
        .205               .5           .07606           .0681453         7.914671
DIFFERENCE CHANGE IN 5MM INTERVAL IS   191.2238 MICRONS
THIS EQUALS A CHANGE OF   302.1868 FRINGES AT .6328 MICRONS
IN THE 5MM INTERVAL
         .3                .5          .0894018          .0778835          11.5183
        .305               .5          .0902213          .0785151          11.7062
DIFFERENCE CHANGE IN 5MM INTERVAL IS 187.899 MICRONS
THIS EQUALS A CHANGE OF   296.9327 FRINGES AT .6328 MICRONS
IN THE 5MM INTERVAL
         .4                .5          .1079848          .0927494         15.23542
        .405               .5          .1090341          .0936153         15.41885
DIFFERENCE CHANGE IN 5MM INTERVAL IS   183.4306 MICRONS
THIS EQUALS A CHANGE OF   289.8713 FRINGES AT .6328 MICRONS
IN THE 5MM INTERVAL
         .5                .5           .131103            .11225         18.85303
        .505               .5          .1323754          .1133445         19.03093
DIFFERENCE CHANGE IN 5MM INTERVAL IS   177.9032 MICRONS
THIS EQUALS A CHANGE OF   281.1365 FRINGES AT .6328 MICRONS
IN THE 5MM INTERVAL
         .6                .5          .1586107          .1362584         22.35226
        .605               .5          .1600984          .1375745         22.52381
DIFFERENCE CHANGE IN 5MM INTERVAL IS 171.555 MICRONS
THIS EQUALS A CHANGE OF   271.1047 FRINGES AT .6328 MICRONS
IN THE 5MM INTERVAL
         .7                .5          .1903424          .1646247         25.71776
        .705               .5          .1920367          .1661544          25.8823
DIFFERENCE CHANGE IN 5MM INTERVAL IS   164.5405 MICRONS
THIS EQUALS A CHANGE OF   260.0198 FRINGES AT .6328 MICRONS
IN THE 5MM INTERVAL
         .8                .5          .2261177            .19718         28.93768
        .805               .5          .2280092          .1989145         29.09469
DIFFERENCE CHANGE IN 5MM INTERVAL IS   157.0134 MICRONS
THIS EQUALS A CHANGE OF   248.1249 FRINGES AT .6328 MICRONS
IN THE 5MM INTERVAL
         .9                .5          .2657449          .2337412         32.00366
        .905               .5          .2678238           .235671         32.15281
DIFFERENCE CHANGE IN 5MM INTERVAL IS   149.1423 MICRONS
THIS EQUALS A CHANGE OF   235.6863 FRINGES AT .6328 MICRONS
IN THE 5MM INTERVAL
```